Abrupt episode of mid-Cretaceous ocean acidification triggered by massive volcanism

Author list

Matthew M. Jones[1,2,*], Bradley B. Sageman[1], David Selby[3], Andrew D. Jacobson[1], Sietske J. Batenburg[4], Laurent Riquier[5], Kenneth G. MacLeod[6], Brian T. Huber[2], Kara A. Bogus[7], Maria Luisa G. Tejada[8], Junichiro Kuroda[9], Richard W. Hobbs[3]

Affiliations

[1]Department of Earth and Planetary Sciences, Northwestern University, Evanston, IL, USA 60208

[2]National Museum of Natural History, Smithsonian Institution, Washington, DC 20560, USA

[3]Dept. of Earth Science, University of Durham, South Road, Durham DH1 3LE, UK

[4]Department de Dinamica de la Terra i de l'Ocea, Universitat de Barcelona, Barcelona, Spain

[5]Institut des Sciences de la Terre de Paris (ISTeP), CNRS, Sorbonne Université, Paris 75005, France

[6]Department of Geological Sciences, University of Missouri, Columbia, MO 65211, USA

[7]Camborne School of Mines, College of Engineering, Math and Physical Sciences, University of Exeter, Penryn, UK

[8]Institute for Marine Geodynamics (IMG), Japan Agency for Marine-Earth Science and Technology, 2-15 Natsushima-cho, Yokosuka-shi, Kanagawa 237-0061, Japan

[9]Department of Ocean Floor GeoScience, University of Tokyo, 5-1-5 Kashiwanoha, Kashiwa, Chiba 277-8564, Japan

*corresponding author; email: matthewjones2012@u.northwestern.edu

Abstract

Large igneous province volcanic activity during the mid-Cretaceous approximately 94.5 million years ago triggered a global-scale episode of reduced marine oxygen levels known as Oceanic Anoxic Event 2. It has been hypothesized that this geologically rapid degassing of volcanic carbon dioxide altered seawater carbonate chemistry, affecting marine ecosystems, geochemical cycles, and sedimentation. Here, we report on two sites drilled by the International Ocean Discovery Program offshore of southwest Australia that exhibit clear evidence for suppressed pelagic carbonate sedimentation in the form of a stratigraphic interval barren of carbonate, recording ocean acidification during the event. We then use the osmium isotopic composition of bulk sediments to directly link this protracted ~600-kiloyear shoaling of the marine calcite compensation depth to the onset of volcanic activity. This decrease in marine pH was prolonged by biogeochemical feedbacks in highly productive regions that elevated heterotrophic respiration of carbon dioxide to the water column. A compilation of mid-Cretaceous marine stratigraphic records reveals a contemporaneous decrease of sedimentary carbonate content at continental slope sites globally. Thus, we contend that changes in marine carbonate chemistry are a primary ecological stress and important consequence of rapid emission of carbon dioxide during many large igneous province eruptions in the geologic past.

Main Text

Introduction

Episodes of ocean acidification in Earth history provide context for predicting the future consequences of anthropogenic CO_2 emissions. Potential geologic acidification events have been identified during the Paleocene-Eocene Thermal Maximum (PETM), end-Permian mass extinction, Triassic-Jurassic boundary, and Mesozoic oceanic anoxic events[1–5]. However, some geologic episodes of prolific volcanic CO_2 release may have occurred too slowly to significantly decrease marine pH[6] given that emission rates must outpace fluxes of alkalinity from silicate weathering and seafloor carbonate dissolution, which buffer ocean carbonate chemistry on timescales of 10's of kiloyears. Therefore, precisely resolved stratigraphic records are key to assessing candidate ocean acidification events. Here, we evaluate the long-standing hypothesis that ocean acidification accompanied the mid-Cretaceous Oceanic Anoxic Event 2 (OAE2, ~94 Ma), ultimately resulting in turnover of marine fauna and altered marine geochemical cycles[7–9].

Ocean acidification's first order effects on marine carbonate chemistry are well understood due to the relationship between pH, alkalinity, carbonate speciation, and carbonate mineral saturation states ($\Omega_{\mathrm{mineral}}$)[10]. However, erosive carbonate dissolution and sediment burndown commonly occur during ocean acidification events, obscuring direct chemostratigraphic proxy records of changes in Ω and pH[5,11]. The stratigraphic record does, however, robustly preserve an alternative marker of ocean acidification in the form of the calcite compensation depth (CCD) – the depth below which pelagic sediments contain low carbonate contents (<20 wt.%) due to calcite undersaturation and dissolution in colder CO_2-rich bottom waters. Rapid addition of CO_2 to the marine realm decreases calcite saturation and forces the CCD to shallow, as is occurring in the modern ocean due to uptake of anthropogenic

CO_2[12]. Thus, paleoacidification events may be identified from punctuated carbonate-barren intervals in pelagic marine strata[1,10,13].

During OAE2, widespread anoxia and euxinia in marine bottom waters led to the deposition of black shales in many, though not all, marine basins globally[14,15]. The organic carbon burial event is defined in stratigraphic records by a positive carbon isotope excursion lasting at least 600 kiloyears across the Cenomanian-Turonian stage boundary [16,17]. A volcanic trigger for OAE2 is suggested by increased contents of volcanogenic elements in marine sediments, and isotopic excursions indicate enhanced activity from large igneous provinces (LIPs) emplaced around the time of the event, such as the Caribbean and/or High Arctic LIPs[7,18] **(Fig. 1a**). Particularly strong evidence for this trigger is a shift to unradiogenic (i.e., mantle-like juvenile volcanic) initial osmium isotope ratios (Os_i) in sediments at many marine sites tens of thousands of years prior to the beginning of OAE2[17,19,20]. Kerr (1998) hypothesized that the Caribbean LIP could have influenced marine carbonate chemistry based on the volume of basalts emplaced (~4×10^6 km^3) and a recent estimate of the total CO_2 degassed during OAE2 ranges from 14,000 to 46,000 Pg of carbon [21]. Additionally, pioneering sedimentological observations of deep-sea cores through the OAE2 interval also noted carbonate barren intervals at many pelagic sites, portending a shallowed CCD[22–25]. Although OAE2 has been implicated in general considerations of acidification through geologic time[4,8], only one recent Ca isotope study has offered direct geochemical evidence for altered calcite saturation states during OAE2[9]. To comprehensively test the OAE2-ocean acidification hypothesis, here we report osmium geochemical proxy evidence for the timing and magnitude of LIP volcanic activity in relation to changes in the CCD preserved in sediment cores from the Mentelle Basin offshore southwest Australia. These osmium data are combined with a compilation of carbonate content records from marine sites to resolve global trends in the CCD during OAE2.

CCD shoaling in the Mentelle Basin. Expedition 369 of the International Ocean Discovery Program (IODP) cored two relatively conformable pelagic successions of OAE2 at Sites U1513 and U1516 in the Mentelle Basin in 2017[26,27] (**Fig. 1a, Extended Data Fig. 1**). At the time of OAE2, these sites were located at ~60°S in the southeastern Tethys Ocean on the subsiding eastern flank of the Naturaliste Plateau at an estimated water depth of ~1100 m[28]. At Site U1516, changing carbonate content[26] and Ca XRF core scanning data reveal a shoaling of the CCD between 471.0-467.3 m rCCSF (revised core composite depth below sea floor) (**Fig. 2**). This 3.7 m thick darker and carbonate-free stratigraphic interval corresponds to much of the encompassing OAE2 interval as constrained by microfossil biostratigraphy and bulk carbonate carbon isotope ($\delta^{13}C_{carb}$) chemostratigraphy[27]. The absence of carbonate minerals means some details of the $\delta^{13}C_{carb}$ excursion (CIE) through the event are not preserved. However, the base and termination of the event's CIE are apparent in the bracketing carbonate-bearing intervals (**Extended Data Fig. 2**). Based on a floating orbital timescale derived from bandpass filtering of Fe XRF core scanning data, the duration of the carbonate compensation event is approximately six short eccentricity cycles, or ~600 kiloyears, which approaches the total duration of the OAE2 CIE at Site U1516 of approximately seven short eccentricity cycles, or ~700 kiloyears [see Methods and **Extended Data Figs. 3-4**].

Extremely unradiogenic Os_i values (<0.2) and high ^{192}Os contents in strata across the base of the OAE2 interval at Site U1516 provide evidence for volcanic activity (**Fig. 2**). The main unradiogenic Os_i excursion (to juvenile volcanic end-member values) and spike in ^{192}Os contents to ~1,800 parts per trillion at Site U1516 both culminate between 471-470 m rCCSF, marking major LIP volcanic activity associated with the onset of OAE2 (**Fig. 2**). This timing is notable because the initial shoaling of the CCD in the Mentelle Basin directly coincides with the geologically rapid intensification of LIP volcanism (**Fig. 3**). Based on inverse modeling of the Os_i and ^{192}Os profiles, the LIP Os flux to the marine reservoir exceeded pre-event baseline mantle/volcanic fluxes by at least 30x during peak intensity and lasting at least 60 kiloyears through the onset of OAE2 [see Methods and **Extended Data Tables 1-2**]. If continental weathering fluxes increased as much as 80% during OAE2 as has been suggested recently[29], the additional radiogenic osmium flux would necessitate an even greater LIP volcanic Os flux approaching 50x baseline levels to recreate the trends in observed Os_i curves (**Extended Data Fig. 5**). Combined, these observations link the emission of volcanically derived CO_2 to the initial shoaling of the CCD at Site U1516 and ocean acidification during OAE2.

More radiogenic (higher) Os_i datapoints and low ^{192}Os contents occur above 469.6 m rCCSF at Site U1516, signaling a waning of LIP volcanic activity in the upper interval of OAE2 roughly 180±60 kiloyears after the start of the event (**Figs. 2-3**). Five unradiogenic Os_i datapoints are intermittently present in this interval (469.4-466.0 m rCCSF) and could possibly represent punctuated renewed LIP eruptions. However, this seems unlikely as the horizons do not record concomitant spikes in ^{192}Os contents and no previously published marine Os_i chemostratigraphic records (n>15) document global-scale LIP volcanic activity in the upper OAE2 or post-OAE2 intervals[17,19,20,30] (**Extended Data Fig. 2**). Thus, it seems more likely these upper unradiogenic Os_i points reflect either seafloor reworking of continental slope sediments or record a localized source of volcanic activity, such as the Kerguelen Plateau, with a smaller Os flux that did not mix on a global scale[31].

Global carbonate sedimentation during OAE2. Trends in marine carbonate sedimentation during OAE2 from a global compilation fall into several categories (**Fig. 1b**). Eight sites from abyssal, continental rise, or lower continental slope settings preserve less than 20 wt.% $CaCO_3$ before, during, and after the OAE2 interval, indicating they remained consistently below or near the CCD. Thirteen sites almost exclusively from epicontinental seas preserve 40-95% $CaCO_3$ prior to and during OAE2 and are therefore interpreted to have remained consistently above the CCD. Of those sites, seven record increases in carbonate content during OAE2. Finally and notably, carbonate contents at thirteen sites mainly from continental slope settings decrease to sub-CCD wt.% $CaCO_3$ values during OAE2 indicating a pronounced shoaling of the CCD in multiple basins globally. The OAE2 interval is relatively condensed at a majority of these shoaled pelagic sites, reflecting reduced carbonate accumulation[32].

Ocean Acidification during OAE2. The observations from our osmium and compiled sedimentological data for OAE2 suggest that ocean acidification was an additional fundamental paleoceanographic response to this episode of LIP volcanism. Acidification resulted in a shoaling of the CCD recorded at continental slope sites globally. In shallower settings through OAE2 though, carbonate deposition progressed and many carbonate platforms persisted [33] despite partial drowning and stress from nutrient loading[34] (**Fig. 1b**). Increases in carbonate content were particularly substantial in epicontinental seaways like the North American Western Interior Seaway, where a pronounced global transgression decreased the relative contribution of siliciclastic sedimentation[35] (**Fig. 1a**). Arthur et al. (1987) attributed carbonate barren deep sea intervals during OAE2 to a shift in carbonate sedimentation from the pelagic realm to the vastly expanded epicontinental seaways. Models invoking sea level rise have successfully recreated prolonged shifts in the CCD through the Middle Eocene

Climatic Optimum "MECO", a rare geologic example of a long-lasting (~500 kiloyears) carbonate compensation event similar to OAE2[36]. Increased shallow marine calcification and consequent decreased alkalinity would have worked in concert with LIP CO_2 emissions to promote shoaling of the CCD during OAE2 in slope marine settings like Site U1516.

The ~600-kiloyear shoaling of the CCD observed during OAE2 at Site U1516 is much longer than predictions of conventional models for marine carbonate chemistry tailored to other geological episodes of voluminous CO_2 release[4]. During the PETM for example, the delivery of alkalinity from seafloor carbonate dissolution and silicate weathering ends surface ocean acidification events within 10s of kiloyears[4]. To reconcile model results and observational data for OAE2, we hypothesize that the remineralization of ample organic carbon sinking from highly productive surfaces waters produced a significant flux of dissolved CO_2 to marine bottom waters. In the lower OAE2 interval at Site U1516, geochemical proxies—such as biogenic Si[37] and Si enrichment factor (Si_{EF}) values—increase near three thin laminated black shale beds (4-12 cm-thick beds labeled "a" "b" "c" in **Fig. 2**), indicating intermittently enhanced primary productivity. In the upper OAE2 interval, more sustained increases in biogenic silica[37], Si_{EF}, and Ba_{EF}, and abundant radiolaria[27], indicate consistently higher productivity levels, which would have led to higher heterotrophic respiration rates and increased dissolved CO_2 in the water column as has been noted previously at OAE2 sites with high total organic carbon (TOC)[38,39]. An intense CO_2 flux from LIP volcanism appears to have triggered ocean acidification, but marine biogeochemical feedbacks that enhanced primary productivity appear to have sustained a shallower CCD for hundreds of kiloyears during OAE2. Differences between model and observation may also reflect that models employ a combination of burndown and continental chemical weathering (chemical compensation) as the dampening mechanism to ocean acidification, whereas Ca isotope data for OAE2[9] and for the older OAE1a[40] point to additional influence from reduced carbonate production (biological compensation)[41].

These marine biogeochemical factors, along with epicontinental carbonate deposition discussed above, would explain the longer duration CCD anomaly during OAE2 and possibly other OAEs[2], especially in comparison to the PETM, an event without pervasive black shale deposition and a positive CIE[1]. Notably, the Site U1516 carbonate record also exhibits a recovery of carbonate deposition following OAE2 (**Fig. 2**). This final deepening of the CCD was likely linked to the factors that ultimately terminated the event, such as alkalinity buildup from reduced carbonate production, increased continental weathering, and/or a decline in global primary productivity, as is observed locally at Site U1516 in waning biogenic silica and Ba_{EF} values above ~467.3 m rCCSF.

Os flux relation with CO_2 release. The relationship between an increasing flux of Os and the emission of CO_2 as LIP activity progressed is poorly constrained and to some degree depends upon the lithology of the intruded host rock[42]. However, if the volcanic Os and C fluxes scaled linearly, a >30x increase in CO_2 emission above background mantle/volcanic degassing rates would begin to approach modern anthropogenic CO_2 emission rates, which are ~80-270x above background volcanic fluxes and are rapidly altering marine carbonate chemistry[12,43]. In the mid-Cretaceous, a scenario of even lower CO_2 release, though of similar order of magnitude and rate, would have strongly affected ocean chemistry due to lower carbonate ion concentrations[10], and would have likely decreased pH and carbonate mineral saturation, as is inferred from Ca isotope records[9] and the shoaled CCD.

Typically, negative CIEs occur during candidate ocean acidification events in the geologic record (e.g., PETM or OAE1a) due to the release of CO_2 with low $\delta^{13}C$ values from volcanogenic carbon reservoirs (~-5‰ PDB or biogenic (<-20‰ PDB - Peedee Belemnite scale)) [1,44]. Near the onset of OAE2, some sites record a negative CIE, possibly reflecting the emission of CO_2 that shoaled the CCD during the event [18,21]. These records are somewhat rare though and could alternatively be explained by local environmental changes in depositional settings that also influence $\delta^{13}C$ values. Somewhat puzzlingly and despite exhibiting a shoaling of the CCD and one of the most severe volcanogenic Os_i excursions of the Phanerozoic, OAE2 is dominantly characterized by a positive CIE [25]. Recently, Mason et al. (2017)[45] showed that volatile-rich volcanic settings which assimilate crustal carbonate also release CO_2 with high $\delta^{13}C$ values (~ -1‰ PDB). Thus, if the volcanism associated with OAE2 erupted in a carbonate-rich setting like the Caribbean (**Fig. 1a**), we hypothesize that CO_2 would have been released from an isotopically heavy pool of C, generating the observed carbonate compensation event independent of a pronounced negative CIE.

Biotic effects of acidification. Marine deoxygenation is hypothesized to have accelerated marine macro- and micro-faunal turnover rates during OAE2[46,47]. Suppressed calcite and aragonite saturation states due to LIP volcanism would also have been a compounding stressor to marine ecosystems. Laboratory studies of modern calcifying organisms record significant declines in calcification rates at $\Omega_{aragonite}$ less than three[48]. Such conditions, where surface waters were not undersaturated and would not experience outright dissolution, but where Ω had declined, are consistent with the epicontinental carbonate sedimentation trends of OAE2. Biotic indicators of ocean acidification, such as dwarfing, thinning, and fragmentation of foraminifera and calcareous nannofossils, occur strikingly during the PETM[11]. Some, but not all, of these features occur during OAE2, in particular, the dwarfing of calcitic microfossils[49,50], which correlates with Ca isotope evidence for reduced precipitation rates[51]. These morphological shifts, along with the extinction of the deep-dwelling, keeled foraminifera *Rotalipora cushmani* early in OAE2, are consistent with a scenario of LIP volcanic CO_2 emission, decreased Ω, global warming, and biotic extinctions[52]. Similarly, records of demise in the mid-Cretaceous rudist reefs[53] along with turnover of aragonitic ammonite[46] and calcitic microfossil[47] taxa may in part record selection following changes in marine carbonate chemistry during OAE2.

Implications and unresolved aspects of mid-Cretaceous ocean acidification. In summary, osmium chemostratigraphic data and compiled sedimentological observations of carbonate content from OAE2 indicate that CO_2 emitted from intense LIP volcanic activity triggered a shoaling of the CCD, which was likely prolonged by subsequent marine biogeochemical feedbacks and sea level transgression. We conclude that ocean acidification represented a notable component of environmental deterioration during OAE2, and perhaps other Mesozoic OAEs, with volcanogenic and biogeochemical fluxes of C to the global ocean that exceeded thresholds for buffering from silicate weathering. In particular, these results raise questions about the temporal relation between shifts in surface water carbonate chemistry and longer duration changes in the CCD during LIP episodes in Earth history. More quantitative depth constraints on the shift of the CCD during OAE2 may help refine the total mass of pelagic carbonate dissolved and, in turn, the amount of CO_2 emitted from LIP sources. However, the relative roles of dissolution versus lower calcification rates[40] in driving the CCD shallower during OAEs must still be quantitatively discerned. As to the source of the CO_2, observations of carbon isotope profiles may fingerprint which volcanic province or provinces were linked to the event, yet the geochronology and eruptive tempo of many mid-Cretaceous LIPs is still coarsely resolved[54] compared with LIPs from other intensely studied intervals, such as the Deccan Traps at the Cretaceous-Paleogene Boundary[55]. Insitu verification of the precise setting and timing of volcanic flows associated with ocean acidification during OAE2 remains a grand challenge in paleoceanography.

These deep-time findings highlight the role that marine nutrient loading, along with elevated productivity and subsequent anoxia, play in exacerbating and prolonging carbonate mineral undersaturation in marine settings. Continued study of how benthic and planktic communities responded to a decrease in calcite saturation state during OAE2 should provide predictive insights into the vulnerabilities and resiliencies of modern ecosystems as marine pH continues to decline. Additional investigations employing existing ocean acidification-sensitive isotope proxies, such as B[4], and emerging ones, including Ca[9] and stable Sr[40], may further critically test for surface water fluctuations in pH, calcite/aragonite saturation, and calcification stress.

Acknowledgements

We are grateful for the dedication of the IODP Expedition 369 Science Party, technicians, and crew in coring Site U1516; analytical support of Antonia Hofmann, Chris Ottley and Geoff Nowell at Durham University; and assistance of Brian Levay with XRF core scanning. This research was funded by a U.S. Science Support Program (USSSP) Post-Expedition Award to MMJ and box modeling and carbonate compilations represent doctoral research of MMJ, partly funded by National Science Foundation Grant 1338312 to BBS. MMJ acknowledges support from the Smithsonian Peter Buck Fellowship; DS acknowledges the TOTAL endowment fund; LR acknowledges support from IODP-France.

Author Contributions

Study conceptualization – M.M.J., B.B.S., A.D.J.; geochemical analyses – M.M.J., D.S., S.J.B., L.R., K.G.M., K.A.B.; field work and core collection – B.T.H., R.W.H., K.A.B., M.L.G.T., J.K., S.J.B., L.R., K.G.M., M.M.J.; original manuscript draft – M.M.J., B.B.S., D.S., A.D.J., K.G.M., S.J.B., L.R.; modeling analyses – M.M.J., S.J.B., M.L.G.T., J.K.; manuscript editing – all.

Competing Interests The authors declare no competing interests.

FIGURE CAPTIONS

Figure 1: A – Late Cretaceous paleomap of sites compiled for carbonate sedimentation through Oceanic Anoxic Event 2 (OAE2). See **Extended Data Table 3** for data sources. Marker colors correspond to paleobathymetric setting and red rings denote sites where a shoaling of the calcite compensation depth (CCD) is observed. Yellow star denotes IODP Site U1516. Purple regions represent Caribbean (CLIP), High Arctic (HALIP), and Kerguelen (KLIP) large igneous provinces. Map adapted from[20]. WIS – Western Interior Seaway. B – A global compilation of trends in sedimentary carbonate contents (wt.%) prior to and during Oceanic Anoxic Event 2 (OAE2). Text color corresponds to paleobathymetric setting. Sites with a precipitous decrease in carbonate during the event record a shoaling CCD (bottom center). Shallow water sites (bottom right) remained above the CCD throughout OAE2 with some increasing in carbonate contents in contrast to deeper water sites (see text for discussion).

Figure 2: Chemostratigraphy and core photos of the Oceanic Anoxic Event 2 (OAE2) interval at IODP Site U1516 (eastern Indian Ocean). LIP volcanism is recorded by a decrease in initial osmium isotope ratios (Os_i; red, panel D) and spike in ^{192}Os contents (ppt=parts per trillion; purple, panel E) near the

base of OAE2. A positive carbonate carbon isotope ($\delta^{13}C_{carb}$, panel C) excursion and nannofossil biostratigraphy [27] confirm this correlation (see **Extended Data Figure 4** for more details). A ~600-kiloyear shoaling of the calcite compensation depth (CCD) is preserved by the near-complete absence of carbonate minerals from ~471-467.3 m rCCSF (revised core composite depth below sea floor) based on shipboard carbonate content data[26] (black dots –panel A) and Ca 10 kV XRF scanning data (blue, panel A). XRF scanning data plotted from cores 3R-5R in Hole D. The bandpass filter of Fe 10 kV XRF scanning data records the short eccentricity orbital cycle of ~100 kyr and forms a floating timescale (panel B). Elemental proxies at right ($Si_{(EF)}$ - silicon enrichment factors, panel F; biogenic Si – biogenic silica[37], panel F; $Ba_{(EF)}$ - barium enrichment factor, panel G) show evidence for increased productivity during OAE2, especially in the upper interval of the event. Together, these data are consistent with a volcanic trigger for ocean acidification and the shoaling of the CCD, which was prolonged by elevated productivity during OAE2.

Figure 3. Inverse modeling results of large igneous province (LIP) volcanic activity during Oceanic Anoxic Event 2 (OAE2; gray shading) based on Os_i (red) and ^{192}Os (purple) data from IODP Site U1516 (circles, panel B). At peak intensity in the OAE2 onset interval, input fluxes of Os from LIP sources (panel A) must be >30 times greater than the global background level of the mid-Cretaceous mantle/volcanic Os flux. The Site U1516 Os_i record is consistent with smaller, yet still significant volcanic activity preceding OAE2 by several hundred kiloyears (kyr). Also plotted is a coeval Os time-series from the Angus Core in the Western Interior Basin of North America[17] (triangles) for a shallow marine comparison (panel B). See Methods for full modeling details.

References

1. Zachos, J. C. Rapid Acidification of the Ocean During the Paleocene-Eocene Thermal Maximum. *Science* **308**, 1611–1615 (2005).
2. Erba, E., Bottini, C., Weissert, H. J. & Keller, C. E. Calcareous Nannoplankton Response to Surface-Water Acidification Around Oceanic Anoxic Event 1a. *Science* **329**, 428–432 (2010).
3. Payne, J. L. *et al.* Calcium isotope constraints on the end-Permian mass extinction. *Proc. Natl. Acad. Sci.* **107**, 8543–8548 (2010).
4. Honisch, B. *et al.* The Geological Record of Ocean Acidification. *Science* **335**, 1058–1063 (2012).
5. Greene, S. E. *et al.* Recognising ocean acidification in deep time: An evaluation of the evidence for acidification across the Triassic-Jurassic boundary. *Earth-Sci. Rev.* **113**, 72–93 (2012).
6. Naafs, B. D. A. *et al.* Gradual and sustained carbon dioxide release during Aptian Oceanic Anoxic Event 1a. *Nat. Geosci.* **9**, 135–139 (2016).
7. Kerr, A. C. Oceanic plateau formation: a cause of mass extinction and black shale deposition around the Cenomanian–Turonian boundary? *J. Geol. Soc.* **155**, 619–626 (1998).
8. Jenkyns, H. C. Geochemistry of oceanic anoxic events: REVIEW. *Geochem. Geophys. Geosystems* **11**, n/a-n/a (2010).
9. Du Vivier, A. D. C. *et al.* Ca isotope stratigraphy across the Cenomanian–Turonian OAE 2: Links between volcanism, seawater geochemistry, and the carbonate fractionation factor. *Earth Planet. Sci. Lett.* **416**, 121–131 (2015).
10. Zeebe, R. E. & Tyrrell, T. History of carbonate ion concentration over the last 100 million years II: Revised calculations and new data. *Geochim. Cosmochim. Acta* **257**, 373–392 (2019).
11. Bralower, T. J. *et al.* Impact of dissolution on the sedimentary record of the Paleocene–Eocene thermal maximum. *Earth Planet. Sci. Lett.* **401**, 70–82 (2014).

12. Sulpis, O. *et al.* Current CaCO3 dissolution at the seafloor caused by anthropogenic CO2. *Proc. Natl. Acad. Sci.* (2018) doi:10.1073/pnas.1804250115.
13. Pälike, H. *et al.* A Cenozoic record of the equatorial Pacific carbonate compensation depth. *Nature* **488**, 609–614 (2012).
14. Schlanger, S. O. & Jenkyns, H. C. Cretaceous Oceanic Anoxic Events: Causes and Consequences. *Geol. En Mijnb.* **55**, 6 (1976).
15. Ostrander, C. M., Owens, J. D. & Nielsen, S. G. Constraining the rate of oceanic deoxygenation leading up to a Cretaceous Oceanic Anoxic Event (OAE-2: ~94 Ma). *Sci. Adv.* **3**, e1701020 (2017).
16. Sageman, B. B., Meyers, S. R. & Arthur, M. A. Orbital time scale and new C-isotope record for Cenomanian-Turonian boundary stratotype. *Geology* **34**, 125 (2006).
17. Jones, M. M. *et al.* Regional chronostratigraphic synthesis of the Cenomanian-Turonian Oceanic Anoxic Event 2 (OAE2) interval, Western Interior Basin (USA): New Re-Os chemostratigraphy and 40Ar/39Ar geochronology. *GSA Bull.* **133**, 1090–1104 (2021).
18. Kuroda, J. *et al.* Contemporaneous massive subaerial volcanism and late cretaceous Oceanic Anoxic Event 2. *Earth Planet. Sci. Lett.* **256**, 211–223 (2007).
19. Turgeon, S. C. & Creaser, R. A. Cretaceous oceanic anoxic event 2 triggered by a massive magmatic episode. *Nature* **454**, 323–326 (2008).
20. Du Vivier, A. D. C. *et al.* Marine 187Os/188Os isotope stratigraphy reveals the interaction of volcanism and ocean circulation during Oceanic Anoxic Event 2. *Earth Planet. Sci. Lett.* **389**, 23–33 (2014).
21. Papadomanolaki, N. M., van Helmond, N. A. G. M., Pälike, H., Sluijs, A. & Slomp, C. P. Quantifying volcanism and organic carbon burial across Oceanic Anoxic Event 2. *Geology* **50**, 511–515 (2022).

22. De Graciansky, P. C. *et al.* The Goban Spur transect: Geologic evolution of a sediment-starved passive continental margin. *GSA Bull.* **96**, 58–76 (1985).
23. Arthur, M. A. & Dean, W. E. Cretaceous paleoceanography of the western North Atlantic Ocean. in *The Western North Atlantic Region* (eds. Vogt, P. R. & Tucholke, B. E.) (Geological Society of America, 1986).
24. Herbin, J. P. *et al.* Organic-rich sedimentation at the Cenomanian-Turonian boundary in oceanic and coastal basins in the North Atlantic and Tethys. *Geol. Soc. Lond. Spec. Publ.* **21**, 389–422 (1986).
25. Arthur, M. A., Schlanger, S. O. & Jenkyns, H. C. The Cenomanian-Turonian Oceanic Anoxic Event, II. Palaeoceanographic controls on organic-matter production and preservation. *Geol. Soc. Lond. Spec. Publ.* **26**, 401–420 (1987).
26. Huber, B. T., Hobbs, R. W., Bogus, K. A. & the Expedition 369 Scientists. Site U1516. in *Australia Cretaceous Climate and Tectonics* (eds. Hobbs, R. W., Huber, B. T. & Bogus, K. A.) vol. 369 (International Ocean Discovery Program, 2019).
27. Petrizzo, M. R. *et al.* Exploring the paleoceanographic changes registered by planktonic foraminifera across the Cenomanian-Turonian boundary interval and Oceanic Anoxic Event 2 at southern high latitudes in the Mentelle Basin (SE Indian Ocean). *Glob. Planet. Change* **206**, 103595 (2021).
28. Lee, E. Y. *et al.* Early Cretaceous subsidence of the Naturaliste Plateau defined by a new record of volcaniclastic-rich sequence at IODP Site U1513. *Gondwana Res.* **82**, 1–11 (2020).
29. Nana Yobo, L., Brandon, A. D., Holmden, C., Lau, K. V. & Eldrett, J. Changing inputs of continental and submarine weathering sources of Sr to the oceans during OAE 2. *Geochim. Cosmochim. Acta* **303**, 205–222 (2021).

30. Li, Y.-X. *et al.* Enhanced ocean connectivity and volcanism instigated global onset of Cretaceous Oceanic Anoxic Event 2 (OAE2) ~94.5 million years ago. *Earth Planet. Sci. Lett.* **578**, 117331 (2022).

31. Jiang, Q., Jourdan, F., Olierook, H. K. H., Merle, R. E. & Whittaker, J. M. Longest continuously erupting large igneous province driven by plume-ridge interaction. *Geology* **49**, 206–210 (2021).

32. de Graciansky, P. C. *et al.* Ocean-wide stagnation episode in the late Cretaceous. *Nature* **308**, 346 (1984).

33. Elrick, M., Molina-Garza, R., Duncan, R. & Snow, L. C-isotope stratigraphy and paleoenvironmental changes across OAE2 (mid-Cretaceous) from shallow-water platform carbonates of southern Mexico. *Earth Planet. Sci. Lett.* **277**, 295–306 (2009).

34. Parente, M. *et al.* Stepwise extinction of larger foraminifers at the Cenomanian-Turonian boundary: A shallow-water perspective on nutrient fluctuations during Oceanic Anoxic Event 2 (Bonarelli Event). *Geology* **36**, 715 (2008).

35. Sageman, B. B., Rich, J., Arthur, M. A., Birchfield, G. E. & Dean, W. E. Evidence for Milankovitch periodicities in Cenomanian-Turonian lithologic and geochemical cycles, western interior USA. *J. Sediment. Res.* **67**, 286–302 (1997).

36. Sluijs, A., Zeebe, R. E., Bijl, P. K. & Bohaty, S. M. A middle Eocene carbon cycle conundrum. *Nat. Geosci.* **6**, 429–434 (2013).

37. Chen, H. *et al.* Enhanced hydrological cycle during Oceanic Anoxic Event 2 at southern high latitudes: New insights from IODP Site U1516. *Glob. Planet. Change* **209**, 103735 (2022).

38. Vogt, P. R. Volcanogenic upwelling of anoxic, nutrient-rich water: A possible factor in carbonate-bank/reef demise and benthic faunal extinctions? *GSA Bull.* **101**, 1225–1245 (1989).

39. Scopelliti, G., Bellanca, A., Neri, R., Baudin, F. & Coccioni, R. Comparative high-resolution chemostratigraphy of the Bonarelli Level from the reference Bottaccione section (Umbria–Marche Apennines) and from an equivalent section in NW Sicily: Consistent and contrasting responses to the OAE2. *Chem. Geol.* **228**, 266–285 (2006).
40. Wang, J., Jacobson, A. D., Sageman, B. B. & Hurtgen, M. T. Stable Ca and Sr isotopes support volcanically triggered biocalcification crisis during Oceanic Anoxic Event 1a. *Geology* (2021) doi:10.1130/G47945.1.
41. Boudreau, B. P., Middelburg, J. J. & Luo, Y. The role of calcification in carbonate compensation. *Nat. Geosci.* **11**, 894–900 (2018).
42. Ganino, C. & Arndt, N. T. Climate changes caused by degassing of sediments during the emplacement of large igneous provinces. *Geology* **37**, 323–326 (2009).
43. Gerlach, T. Volcanic versus anthropogenic carbon dioxide. *Eos Trans. Am. Geophys. Union* **92**, 201–202 (2011).
44. Bauer, K. W., Zeebe, R. E. & Wortmann, U. G. Quantifying the volcanic emissions which triggered Oceanic Anoxic Event 1a and their effect on ocean acidification. *Sedimentology* **64**, 204–214 (2017).
45. Mason, E., Edmonds, M. & Turchyn, A. V. Remobilization of crustal carbon may dominate volcanic arc emissions. *Science* **357**, 290–294 (2017).
46. Elder, W. P. Molluscan extinction patterns across the Cenomanian-Turonian Stage boundary in the Western Interior of the United States. *Paleobiology* **15**, 299–320 (1989).
47. Leckie, R. M., Bralower, T. J. & Cashman, R. Oceanic anoxic events and plankton evolution: Biotic response to tectonic forcing during the mid-Cretaceous. *Paleoceanography* **17**, (2002).

48. Ries, J. B., Cohen, A. L. & McCorkle, D. C. Marine calcifiers exhibit mixed responses to CO2-induced ocean acidification. *Geology* **37**, 1131–1134 (2009).

49. Coccioni, R. & Luciani, V. PLANKTONIC FORAMINIFERA AND ENVIRONMENTAL CHANGES ACROSS THE BONARELLI EVENT (OAE2, LATEST CENOMANIAN) IN ITS TYPE AREA: A HIGH-RESOLUTION STUDY FROM THE TETHYAN REFERENCE BOTTACCIONE SECTION (GUBBIO, CENTRAL ITALY). *J. Foraminifer. Res.* **34**, 109–129 (2004).

50. Faucher, G., Erba, E., Bottini, C. & Gambacorta, G. Calcareous nannoplankton response to the latest Cenomanian Oceanic Anoxic Event 2 perturbation. *Riv. Ital. Paleontol. E Stratigr. Res. Paleontol. Stratigr.* **123**, (2017).

51. Kitch, G. D. *et al.*, Calcium isotope ratios of malformed foraminifera reveal biocalcification stress preceded Oceanic Anoxic Event 2. *Communications Earth & Environment* (in press).

52. Coccioni, R., Sideri, M., Frontalini, F. & Montanari, A. The Rotalipora cushmani extinction at Gubbio (Italy): Planktonic foraminiferal testimonial of the onset of the Caribbean large igneous province emplacement? *Geol Soc Am Spec Pap* **524**, 79–96 (2016).

53. Philip, J. M. & Airaud-Crumiere, C. The demise of the rudist-bearing carbonate platforms at the Cenomanian/Turonian boundary: a global control. *Coral Reefs* **10**, 115–125 (1991).

54. Kasbohm, J., Schoene, B. & Burgess, S. Radiometric Constraints on the Timing, Tempo, and Effects of Large Igneous Province Emplacement. in *Large Igneous Provinces* 27–82 (American Geophysical Union (AGU), 2021). doi:10.1002/9781119507444.ch2.

55. Sprain, C. J. *et al.* The eruptive tempo of Deccan volcanism in relation to the Cretaceous-Paleogene boundary. *Science* **363**, 866–870 (2019).

Methods

Astrochronologic time scale construction

The Cenomanian–Turonian sediments at IODP Site U1516 display a rhythmic banding pattern of dark and light lithologies (see Core Photos) that is particularly well expressed around 477 m[26]. Here, the darker bands occur at a scale of ~20 cm, and vary in darkness on a scale of 80 cm to 1 m. This may reflect the influence of eccentricity-modulated precession, with individual (~20 cm scale) alternations corresponding to precession cycles and the bundling corresponding to the influence of the short eccentricity (~100 kyr) cycle.

REDFIT power spectra[56] of the Fe core-scanning XRF data of three stratigraphic intervals (the carbonate-free interval and the intervals above and below) confirm the detection of these periodicities (**Extended Data Figure 3**). Additionally, they exhibit a decrease in sedimentation rate over the carbonate-free interval attributed to the shoaling of the CCD. Dominant periodicities were extracted by band-pass filtering in AnalySeries[57], with a frequency of 1.24 cycles/m and a bandwidth of 0.41 for the intervals above and below the carbonate-free interval, and with a frequency of 1.90 cycles/m and a bandwidth of 0.63 for the carbonate-free interval.

Osmium isotope modeling of volcanic activity

Principles: To quantitatively assess the magnitude and rate of LIP volcanic activity during OAE2, we implemented an osmium isotope box model following the approach of Tejada et al. (2009)[58]. The marine Os isotopic reservoir is highly sensitive to changes in unradiogenic volcanic fluxes ($^{187/188}$Os = 0.126) relative to radiogenic fluxes of continental weathering ($^{187/188}$Os = ~1.4, global average)[59].

Moreover, the marine osmium reservoir has a short residence time (10's of kyr) and was relatively well-mixed during Mesozoic OAEs. As a result, the Os_i chemostratigraphic records of OAE2 from marine sites globally exhibit rapid perturbations from mantle-sourced Os originating from LIPs[17,19,20,30,60–62].

We use a simple inverse model to reconstruct the first-order trends in the OAE2 Os_i excursion and ^{192}Os concentration time-series at IODP Site U1516 (Figure 3). The Site U1516 Os_i and ^{192}Os time-series were generated from the site's short-eccentricity bandpass astronomical time scale, using the 'tune' function in R-package 'Astrochron' [63]. In addition we plot the densely sampled, conformable, and astronomically-tuned Os time series from the Angus Core in the Western Interior Seaway of North America[17] for comparison. Model calculations were performed using MATLAB and R scripts available upon request.

Parameterization: The box model calculates the mass (M_o) and isotopic composition (R_o) of the Late Cretaceous global oceanic osmium reservoir through OAE2 based on input and output fluxes of Os with different isotopic compositions, represented in the following equations:

$$dM_O = F_{riv} + F_{mantle} + F_{cosmic} + F_{LIP} - F_{sed}$$

$$dR_O = \frac{[(F_{riv}*(R_{riv}-R_O))+(F_{mantle}*(R_{mantle}-R_O))+(F_{LIP}*(R_{LIP}-R_O))+(F_{cosmic}(R_{cosmic}-R_O))]}{M_O}$$

Guided by values in[58], the model establishes background input of Os to the ocean from fluxes of unradiogenic cosmic (F_{cosmic}), unradiogenic volcanic/mantle (F_{mantle}), and radiogenic continental weathering/riverine (F_{riv}), along with an output sedimentary flux (F_{sed}) (**Extended Data Table 1**). Osmium isotopic compositions are from [64]. To reconstruct the pre-OAE2 Os_i steady-state value of ~0.75 at Site U1516 in the mid-Cretaceous, F_{mantle} is set at 352 tonnes/kyr (15% less than[58] and F_{riv} is set at 339 tonnes/kyr (15% higher than Tejada et al., 2009[58]). Given likely changes in marine Os cycling between the modeled Early Cretaceous data[58] and the Late Cretaceous data modeled in this study, the minor offsets of our flux values with those in Tejada et al. (2009)[58] are considered reasonable. The model runs for 3000 kyr at a step of 1 kyr. For the purpose of comparing the model results to the measured sedimentary Os_i datasets, time zero (t=0) is aligned to the datapoint in each chemostratigraphic record that is prior to the earliest extremely unradiogenic Os_i value ($Os_i < 0.3$) indicative of intense LIP activity. The model is permitted to run for several hundred kiloyears prior to the oldest measured Os datapoint to reach a steady state.

Large igneous province perturbation: The model also incorporates a perturbation flux representing the flux of unradiogenic Os to the global ocean from LIP volcanic activity (F_{LIP}) during OAE2, presumably from a submarine setting. In an inverse approach and holding all background Os input fluxes constant (F_{riv}, F_{mantle}, F_{cosmic}), the F_{LIP} was iteratively adjusted at 11 control points through time to generate a marine $^{187/188}$Os composition that approximated the general trends in U1516 Os time-series (Fig. 3; **Extended Data Table 2**). F_{LIP} values were linearly interpolated between these control points using the 'interp1' function in MATLAB to create a continuous perturbation scenario, varying through time. Highly unradiogenic Os_i datapoints in the upper OAE2 to post-OAE2 intervals at Site U1516 were interpreted as likely unrepresentative of a globally correlative increase in F_{LIP} for several reasons (see main text). Therefore, iterative modeling of LIP volcanic activity did not attempt to recreate these anomalies.

Re-Os analytical methods

Samples from IODP Site U1516 were analyzed for rhenium-osmium geochemistry (n=28; 463.00 – 480.04 m rCCSF) to establish chemostratigraphic markers of LIP volcanic activity associated with OAE2. Sampling depth resolution ranged from 17-205 cm/sample spanning the Cenomanian-Turonian boundary stratigraphic interval, with higher sampling density in the OAE2 interval. Data are reported in **Supplementary Table 1**.

Prior to analysis at Durham University, samples were powdered in ceramic containers using high-purity crushing techniques at Northwestern University and the University of Michigan. The ceramic containers were cleaned using Ottawa sand, then washed and finally rinsed with ethanol. The prepared powders were analyzed in the Source Rock and Sulfide Geochronology and Geochemistry Laboratory at Durham University utilizing isotope dilution negative ion mass spectrometry[65]. In brief, sample powders (0.3–1.0 g) were spiked with a mixed ^{185}Re+^{190}Os tracer solution and digested in sealed Carius tubes with 8 mL of 0.25 g/g CrO_3 in 4N H_2SO_4 for ~48 hours at 220°C, principally leaching hydrogenous Re and Os (i.e., carbonates and organic matter). The Os fraction was isolated and purified via chloroform extraction with back reduction into HBr and $CrO_3 \cdot H_2SO_4$-HBr microdistillation. The Re fraction was isolated via NaOH-acetone extraction and anion chromatography. Isotopic ratios of samples and solution standards (Re STD and DROs) were measured on a Thermo Triton thermal ionization mass spectrometer (TIMS) in negative ionization mode in the Arthur Holmes Laboratory at Durham University. Running average values for ^{187}Os/^{188}Os and ^{187}Re/^{185}Re solution standards to the time of these analyses (10/2019) were 0.16094±0.00050 (1 σ; n = 700) and 0.59861±0.00159 (1 σ; n = 506), respectively. Total procedural blanks during this study were 15.5 ± 3.5 pg and 0.08 ± 0.03 pg (1σ S.D., n = 3) for Re and Os, respectively, with an average ^{187}Os/^{188}Os value of 0.21 ± 0.01 (n = 3). Present-day measured ^{187}Os/^{188}Os values of samples were corrected to initial osmium ratios (Os_i) by accounting for post-depositional beta decay of ^{187}Re ($\lambda = 1.666 \times 10^{-11} \text{yr}^{-1}$ [66]) using an age of 94.0 Ma for the Cenomanian-Turonian stage boundary[17].

XRF core scanning methods

Split section halves of cores from Site U1516 were analyzed on two Avaatech X-ray fluorescence (XRF) scanners in the XRF Core Scanning Facility at the IODP Gulf Coast Repository in College Station, Texas in 2018. Section halves spanning the OAE2 stratigraphic interval were scanned from Hole C and Hole D (Cores 2R-5R). Emission of secondary fluoresced X-rays characteristic to a suite of elements were generated from scanning at excitation energy levels of 10, 30, and 50 kV. These scans measured chemostratigraphic records of semi-quantitative elemental concentrations in units of counts per second at a median depth sampling resolution of 1.5 cm. Counts of Ca, Fe, and Si are reported from the 10 kV scan (no filter, 0.160 mA). Counts of Ba are reported from the 50 kV scan (Cu filter, 0.75 mA). Full details on XRF scanning methods are presented in Bogus et al. (2019)[67]. Processed scanning data can be accessed at the IODP online repository (https://web.iodp.tamu.edu/LORE/). We interpret Ca XRF scanning data to primarily reflect the relative carbonate mineral (calcite) contents of cores given its correlation with shipboard wt. percent carbonate content data (**Figure 2**).

Major and minor element analytical methods

Prior to analysis, bulk-rock samples were powdered to ~10 μm using a ring and puck mill at Sorbonne University's ISTeP laboratory (Paris, France). Concentration of Si and Ba were determined respectively with an ICP-OES (Thermo Fisher iCap 6500) and an ICP-MS (7700X Agilent) at the spectrochemical laboratory of the Service d'Analyse des Roches et des Minéraux (SARM) of the Centre National de la Recherche Scientifique (CNRS; Vandoeuvre-les-Nancy, France). Sample powder preparation consisted of fusion with $LiBO_2$, followed by acid digestion in HNO_3 (2%) [68]. Precision and accuracy are both better than 1% for Si and 5% for Ba, respectively.

Sedimentary Si and Ba contents are considered paleoproductivity proxies in many marine settings[37,69]. To account for the influence of carbonate non-deposition on elemental abundances during OAE2, enrichment factors (EF) were calculated for the elements Si and Ba at Site U1516. For a given element of interest, enrichment factors calculate the ratio of a sample's elemental content to its Al content and normalize that ratio to a reference value, using the following equation[69]:

$EF = \frac{\left(\frac{element}{Al}\right)_{sample}}{\left(\frac{element}{Al}\right)_{average\ shale}}$ Various reference datasets exist. For this work, the EFs were calculated using the Upper Continental Crust (UCC) reference shale[70].

Global OAE2 carbonate content compilation

Values for sedimentary weight percent carbonate contents in the pre-OAE2 and OAE2 intervals reported in the global compilation are estimated averages from studies with quantitative data [22,26,71–107].

Code Availability Statement: Matlab and R codes for inverse box modeling of isotopic records are available as a Zenodo data repository item (10.5281/zenodo.7182186).

Data Availability Statement: All geochemical data measured for this study are available as a Zenodo data repository item (10.5281/zenodo.7182186). Core scanning X-ray fluorescence (XRF) data for Site U1516 are available through the International Ocean Discovery Program (IODP) at web.iodp.tamu.edu/LORE/.

Correspondence and request for materials should be directed to M.M.J.

Methods-only references

56. Schulz, M. & Mudelsee, M. REDFIT: estimating red-noise spectra directly from unevenly spaced paleoclimatic time series. *Comput. Geosci.* **28**, 421–426 (2002).
57. Paillard, D., Labeyrie, L. & Yiou, P. Macintosh Program performs time-series analysis. *Eos Trans. Am. Geophys. Union* **77**, 379–379 (1996).
58. Tejada, M. L. G. *et al.* Ontong Java Plateau eruption as a trigger for the early Aptian oceanic anoxic event. *Geology* **37**, 855–858 (2009).
59. Peucker-Ehrenbrink, B. & Ravizza, G. The marine osmium isotope record. *Terra Nova* **12**, 205–219 (2000).
60. Du Vivier, A. D. C., Selby, D., Condon, D. J., Takashima, R. & Nishi, H. Pacific 187 Os/ 188 Os isotope chemistry and U–Pb geochronology: Synchroneity of global Os isotope change across OAE 2. *Earth Planet. Sci. Lett.* **428**, 204–216 (2015).
61. Schröder-Adams, C. J., Herrle, J. O., Selby, D., Quesnel, A. & Froude, G. Influence of the High Arctic Igneous Province on the Cenomanian/Turonian boundary interval, Sverdrup Basin, High Canadian Arctic. *Earth Planet. Sci. Lett.* **511**, 76–88 (2019).

62. Sullivan, D. L. *et al.* High resolution osmium data record three distinct pulses of magmatic activity during cretaceous Oceanic Anoxic Event 2 (OAE-2). *Geochim. Cosmochim. Acta* **285**, 257–273 (2020).

63. Meyers, S. R. Astrochron: An R Package for Astrochronology. http://cran.r-project.org/package=astrochron (2014).

64. Levasseur, S., Birck, J. L. & Allegre, C. J. The osmium riverine flux and the oceanic mass balance of osmium. *Earth Planet. Sci. Lett.* **174**, 7–23 (1999).

65. Selby, D. & Creaser, R. A. Re-Os geochronology of organic rich sediments: an evaluation of organic matter analysis methods. *Chem. Geol.* **200**, 225–240 (2003).

66. Smoliar, M. I., Walker, R. J. & Morgan, J. W. Re-Os ages of group IIA, IIIA, IVA, and IVB iron meteorites. *Science* **271**, 1099–1102 (1996).

67. Bogus, K. A. *et al.* Shore-based X-ray fluorescence core scanning of IODP Expedition 369 (Australia Cretaceous Climate and Tectonics) material. in *Australia Cretaceous Climate and Tectonics* vol. 369 (2019).

68. Carignan, J., Hild, P., Mevelle, G., Morel, J. & Yeghicheyan, D. Routine Analyses of Trace Elements in Geological Samples using Flow Injection and Low Pressure On-Line Liquid Chromatography Coupled to ICP-MS: A Study of Geochemical Reference Materials BR, DR-N, UB-N, AN-G and GH. *Geostand. Geoanalytical Res.* **25**, 187–198 (2001).

69. Brumsack, H.-J. The trace metal content of recent organic carbon-rich sediments: Implications for Cretaceous black shale formation. *Palaeogeogr. Palaeoclimatol. Palaeoecol.* **232**, 344–361 (2006).

70. McLennan, S. M. Relationships between the trace element composition of sedimentary rocks and upper continental crust. *Geochem. Geophys. Geosystems* **2**, (2001).

71. Tucholke, B. E. *et al.* Site 387; Cretaceous to Recent sedimentary evolution of the western Bermuda Rise. in *Initial Reports of the Deep Sea Drilling Project* vol. 43 (Texas A & M University, Ocean Drilling Program, College Station, TX, United States, 1979).
72. Arthur, M. A. North Atlantic Cretaceous Black Shales: The Record at Site 398 and a Brief Comparison with Other Occurrences. in *Initial Reports of the Deep Sea Drilling Project* (eds. Sibuet, J.-C. & Ryan, W. B. F.) vol. 47 719–751 (U.S. Government Printing Office, 1979).
73. Meyers, P. A. Appendix II. Organic carbon and calcium carbonate analyses, Deep Sea Drilling Project Leg 93, North American continental rise. in *Initial Reports, DSDP, 93* (eds. van Hinte, J. E. & Wise, S. W.) vol. 93 465–469 (U.S. Government Printing Office, 1987).
74. Dean, W. E. & Arthur, M. A. 46. Inorganic and organic geochemistry of Eocene to Cretaceous strata recovered from the lower continental rise, North American Basin, Site 603, Deep Sea Drilling Project Leg 93. in *Initial Reports of the Deep Sea Drilling Project* vol. 93 1093–1137 (1987).
75. Herbin, J. P., Masure, E. & Roucache, J. Cretaceous Formations from the Lower Continental Rise off Cape Hatteras: Organic Geochemistry, Dinoflagellate Cysts, and the Cenomanian/Turonian Boundary Event at Sites 603 (Leg 93) and 105 (Leg 11). in *Initial Reports of the Deep Sea Drilling Project* (eds. van Hinte, J. E. & Wise, S. W.) vol. 93 1139–1162 (U.S. Government Printing Office, 1987).
76. Cameron, D. H. Grain-Size and Carbon/Carbonate Analyses, Leg43. in *Initial Reports of the Deep Sea Drilling Project* vol. 43 1043–1047 (U.S. Government Printing Office, 1979).
77. van Helmond, N. A. G. M., Ruvalcaba Baroni, I., Sluijs, A., Sinninghe Damsté, J. S. & Slomp, C. P. Spatial extent and degree of oxygen depletion in the deep proto-North Atlantic basin during Oceanic Anoxic Event 2. *Geochem. Geophys. Geosystems* **15**, 4254–4266 (2014).

78. Forster, A. *et al.* The Cenomanian/Turonian oceanic anoxic event in the South Atlantic: New insights from a geochemical study of DSDP Site 530A. *Palaeogeogr. Palaeoclimatol. Palaeoecol.* **267**, 256–283 (2008).

79. Huber, B. T. Middle–Late Cretaceous climate of the southern high latitudes: Stable isotopic evidence for minimal equator-to-pole thermal gradients. *Geol. Soc. Am. Bull.* 28 (1995).

80. Uchman, A., Bąk, K. & Rodríguez-Tovar, F. J. Ichnological record of deep-sea palaeoenvironmental changes around the Oceanic Anoxic Event 2 (Cenomanian–Turonian boundary): An example from the Barnasiówka section, Polish Outer Carpathians. *Palaeogeogr. Palaeoclimatol. Palaeoecol.* **262**, 61–71 (2008).

81. Huber, B. T., Hobbs, R. W., Bogus, K. A. & and the Expedition 369 Scientists. Site U1513. in *Proceedings of the International Ocean Discovery Program* vol. 369 (2019).

82. Thurow, J., Brumsack, H. J., Rullkotter, J., Littke, R. & Meyers, P. A. The Cenomanian-Turonian Boundary event in the Indian Ocean - a key to understand the global picture. in *Synthesis of Results from Scientific Drilling in the Indian Ocean* (eds. Duncan, R. A., Rea, D. K., Kidd, R. B., von Rad, U. & Weissel, J. K.) vol. 70 253–274 (American Geophysical Union, 1992).

83. Rullkötter, J. *et al.* Petrography and geochemistry of organic matter in Triassic and Cretaceous deep-sea sediments from the Wombat and Exmouth plateaus and nearby abyssal plains off northwest Australia. in *Proceedings of the Ocean Drilling Program, Scientific Results* (eds. Von Rad, U. & Haq, B. U.) vol. 122 317–333 (Ocean Drilling Program, 1992).

84. Thurow, J. *et al.* The Cenomanian/Turonian Boundary Event (CTBE) at Hole 641A, ODP Leg 103 (Compared with the CTBE interval at Site 398). in *Proceeding of the Ocean Drilling Program, Scientific Results* (eds. Boillot, G. & Winterer, E. L.) vol. 103 587–634 (Ocean Drilling Program, 1988).

85. Shipboard Scientific Party. Leg 207 summary. in *Proc. ODP, Init. Repts.* (eds. Erbacher, J., Mosher, D. C. & Malone, M. J.) 1–89 (2004).

86. Sinninghe Damsté, J. S., van Bentum, E. C., Reichart, G.-J., Pross, J. & Schouten, S. A CO2 decrease-driven cooling and increased latitudinal temperature gradient during the mid-Cretaceous Oceanic Anoxic Event 2. *Earth Planet. Sci. Lett.* **293**, 97–103 (2010).

87. Arnaboldi, M. & Meyers, P. A. Data report: multiproxy geochemical characterization of OAE-related black shales at Site 1276, Newfoundland Basin. in *Proc. ODP, Sci. Results* (eds. Tucholke, B. E., Sibuet, J.-C. & Klaus, A.) vol. 210 1–18 (2006).

88. Hetzel, A., Boettcher, M. E., Wortmann, U. G. & Brumsack, H.-J. Paleo-redox conditions during OAE 2 reflected in Demerara Rise sediment geochemistry (ODP Leg 207). *Palaeogeogr. Palaeoclimatol. Palaeoecol.* **273**, 302–328 (2009).

89. Waples, D. W. & Cunningham, R. Leg 80 Shipboard Organic Geochemistry. in *Initial Reports Deep Sea Drilling Program* (eds. de Graciansky, P. C. & Poag, C. W.) vol. 80 949–968 (U.S. Government Printing Office, 1985).

90. Wagreich, M., Bojar, A.-V., Sachsenhofer, R. F., Neuhuber, S. & Egger, H. Calcareous nannoplankton, planktonic foraminiferal, and carbonate carbon isotope stratigraphy of the Cenomanian–Turonian boundary section in the Ultrahelvetic Zone (Eastern Alps, Upper Austria). *Cretac. Res.* **29**, 965–975 (2008).

91. Turgeon, S. & Brumsack, H.-J. Anoxic vs dysoxic events reflected in sediment geochemistry during the Cenomanian–Turonian Boundary Event (Cretaceous) in the Umbria–Marche Basin of central Italy. *Chem. Geol.* **234**, 321–339 (2006).

92. Linnert, C., Mutterlose, J. & Herrle, J. O. Late Cretaceous (Cenomanian–Maastrichtian) calcareous nannofossils from Goban Spur (DSDP Sites 549, 551): Implications for the palaeoceanography of the proto North Atlantic. *Palaeogeogr. Palaeoclimatol. Palaeoecol.* **299**, 507–528 (2011).
93. Exon, N. F., Borella, P. E. & Ito, M. Sedimentology of marine Cretaceous sequences in the central Exmouth Plateau (northwest Australia). in *Proceedings of the Ocean Drilling Program* (eds. von Rad, U. & Haq, B. U.) vol. 122 233–257 (U.S. Government Printing Office, 1992).
94. Meyers, P. A., Yum, J.-G. & Wise, S. W. Origins and maturity of organic matter in mid-Cretaceous black shales from ODP Site 1138 on the Kerguelen Plateau. *Mar. Pet. Geol.* **26**, 909–915 (2009).
95. Dickson, A. J. *et al.* A Southern Hemisphere record of global trace-metal drawdown and orbital modulation of organic-matter burial across the Cenomanian–Turonian boundary (Ocean Drilling Program Site 1138, Kerguelen Plateau). *Sedimentology* **64**, 186–203 (2017).
96. Huber, B. T., Leckie, R. M., Norris, R. D., Bralower, T. J. & CoBabe, E. Foraminiferal assemblage and stable isotopic change across the Cenomanian-Turonian boundary in the subtropical North Atlantic. *J. Foraminifer. Res.* **29**, 392–417 (1999).
97. Bowman, A. R. & Bralower, T. J. Paleoceanographic significance of high-resolution carbon isotope records across the Cenomanian–Turonian boundary in the Western Interior and New Jersey coastal plain, USA. *Mar. Geol.* **217**, 305–321 (2005).
98. Joo, Y. J. & Sageman, B. B. Cenomanian To Campanian Carbon Isotope Chemostratigraphy from the Western Interior Basin, U.S.A. *J. Sediment. Res.* **84**, 529–542 (2014).
99. Bomou, B. *et al.* The expression of the Cenomanian–Turonian oceanic anoxic event in Tibet. *Palaeogeogr. Palaeoclimatol. Palaeoecol.* **369**, 466–481 (2013).

100. Sageman, B. B., Lyons, T. W. & Joo, Y. Ji. Geochemistry of Fine-Grained, Organic Carbon-Rich Facies. in *Treatise on Geochemistry* 141–179 (Elsevier, 2014). doi:10.1016/B978-0-08-095975-7.00706-3.

101. Wendler, J. E., Lehmann, J. & Kuss, J. Orbital time scale, intra-platform basin correlation, carbon isotope stratigraphy and sea-level history of the Cenomanian–Turonian Eastern Levant platform, Jordan. *Geol. Soc. Lond. Spec. Publ.* **341**, 171–186 (2010).

102. Paez-Reyes, M. *et al.* Assessing the contribution of the La Luna Sea to the global sink of organic carbon during the Cenomanian-Turonian Oceanic Anoxic Event 2 (OAE2). *Glob. Planet. Change* **199**, 103424 (2021).

103. Nederbragt, A. J. & Fiorentino, A. Stratigraphy and palaeoceanography of the Cenomanian-Turonian Boundary Event in Oued Mellegue, north-western Tunisia. *Cretac. Res.* **20**, 47–62 (1999).

104. Voigt, S., Gale, A. S. & Voigt, T. Sea-level change, carbon cycling and palaeoclimate during the Late Cenomanian of northwest Europe; an integrated palaeoenvironmental analysis. *Cretac. Res.* **27**, 836–858 (2006).

105. Beil, S. *et al.* New insights into Cenomanian paleoceanography and climate evolution from the Tarfaya Basin, southern Morocco. *Cretac. Res.* **84**, 451–473 (2018).

106. Takashima, R. *et al.* Litho-, bio- and chemostratigraphy across the Cenomanian/Turonian boundary (OAE 2) in the Vocontian Basin of southeastern France. *Palaeogeogr. Palaeoclimatol. Palaeoecol.* **273**, 61–74 (2009).

107. Peryt, D. & Wyrwicka, K. The Cenomanian/Turonian boundary event in Central Poland. *Palaeogeogr. Palaeoclimatol. Palaeoecol.* **104**, 185–197 (1993).

108. Huber, B. T., Hobbs, R. W., Bogus, K. A. & the Expedition 369 Science Party. Expedition 369 summary. in *Australia Cretaceous Climate and Tectonics* (eds. Hobbs, R. W., Huber, B. T., Bogus, K. A. & the Expedition 369 Scientists) (2019).

109. Bralower, T. J. Calcareous nannofossil biostratigraphy and assemblages of the Cenomanian-Turonian boundary interval: Implications for the origin and timing of oceanic anoxia. *Paleoceanography* **3**, 275–316 (1988).

Extended Data Figure 1. Map of International Ocean Discovery Program (IODP) Site U1516 (yellow circle). Additional sites cored during IODP Expedition 369 in the Mentelle Basin offshore southwest Australia are displayed (modified from [108]). Bathymetric contour interval of 500 meters. DSDP = Deep Sea Drilling Program.

Extended Data Figure 2. Stratigraphic correlation of the Cenomanian-Turonian boundary interval at IODP Site U1516 to the Portland Core near the base Turonian Global Stratotype Section and Point (GSSP) in Colorado, USA. Oceanic Anoxic Event 2 (OAE2) is defined by a positive carbon isotope ($\delta^{13}C$) excursion (grey shading). The correlation is based on: 1) the base and termination of the $\delta^{13}C$ excursion[27], 2) the anomalously high ^{192}Os abundance interval (light purple dashed line) linked to large igneous province (LIP) volcanic activity[19], 3) the base of the initial osmium isotope ($^{187/188}Os_i$) excursion associated with LIP volcanism at the base of OAE2[19], and 4) bandpassed ~100 kyr-short eccentricity cycles. Calcareous nannofossil biostratigraphy independently supports the correlation as the CC10a/CC10b subzone boundary, approximated by the last occurrence (LO) of *Axopodorhabdus albianus*, falls in the carbonate barren interval at Site U1516[27] and lower OAE2 interval in Portland Core[109]. Site U1516 data sources: $\delta^{13}C$ data[27], Os data and and cyclostratigraphy (this study). Portland Core data sources: Os data[20], $\delta^{13}C$ data[16] (figure adapted from[17]). kcps =

kilocounts per second; VPDB = Vienna Peedee Belemnite scale; ppt = parts per trillion; CCD = calcite compensation depth.

Extended Data Figure 3. REDFIT power spectra of Fe XRF scanning data from IODP Site U1516. Plots span intervals of A: 455.2–467.4 m rCCSF; B: 467.4–470.7 m rCCSF and C: 470.7–481.8 m rCCSF, using a Welch window with 80%, 90%, 95% and 99% confidence levels, and main periodicities indicated.

Extended Data Figure 4. Floating astrochronology for the Cenomanian-Turonian boundary interval at IODP Site U1516. This is based on a short eccentricity bandpass ~100-kyr filter of the cyclic Fe XRF scanning data from Hole D. Squares in right pane show sedimentation rate estimates from the bandpass filter and dashed line shows an average sedimentation rate of 0.8 cm/kyr for the general interval from shipboard nannofossil biostratigraphy[26]. The unradiogenic Os_i excursion marks the onset of LIP volcanism several tens of kiloyear before the initiation of the OAE2 carbon isotope excursion in most conformable sites[17,19,20,60,61]. The base of the Os_i excursion has been dated to 94.55 ± 0.1 Ma[17] and ~94.9 Ma[62], providing scenarios for absolute numerical age tie points for the Site U1516 record.

Extended Data Figure 5. Additional plot of box modeling results for marine $^{187/188}$Os. This includes the scenario of large igneous province (LIP) volcanism (top panel, A) and a second scenario (bottom panel, B) where fluxes of radiogenic osmium from continental weathering (F_{riv}) are set to increase by 80% for 500 kiloyears through Ocean Anoxic Event 2 (OAE2)[29]. An increase in F_{riv} necessitates an even larger increase in the flux of unradiogenic osmium from large igneous province sources (F_{LIP}) by as much as 50x larger than background mantle/volcanic fluxes. Model outputs are plotted against initial osmium isotope ratio data (Os_i) through OAE2 from IODP Site U1516 in the

Indian Ocean (circle symbols and dotted line, this study) and the Angus Core in the Western Interior Basin of North America[17].

Extended Data Table 1. Model parameters for Late Cretaceous marine Os fluxes and model initial conditions. See **Extended Data Table 2** for final modeled F_{LIP} values through time.

Extended Data Table 2. Modeled large igneous province Os flux (F_{LIP}) values through time used to perturb the marine Os reservoir during OAE2. F_{LIP} values are reported as a ratio to the background global volcanic/mantle flux (F_{mantle}) (i.e., F_{LIP}/F_{mantle}). For example, a F_{LIP} value of 1.0 represents a large igneous province Os flux as large as the pre-event background volcanic/mantle Os flux.

Extended Data Table 3. A global compilation of carbonate contents (wt.% CaCO3) pre-OAE2 and during OAE2 from 46 sites. Sites in compilation are mapped in **Figure 1a**.

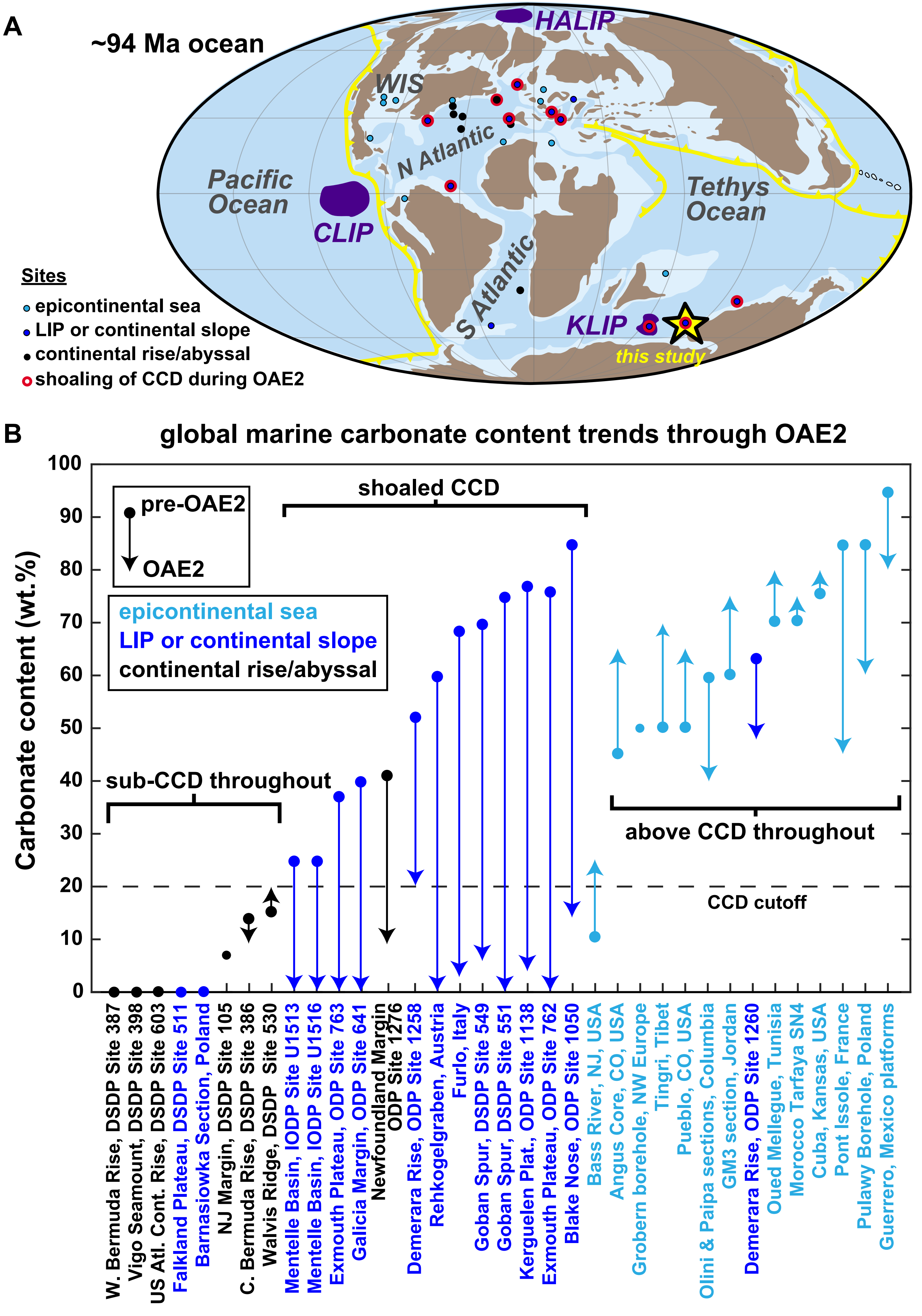
A
~94 Ma ocean
HALIP
WIS
N Atlantic
Pacific Ocean
CLIP
Tethys Ocean
S Atlantic
KLIP
this study
Sites
epicontinental sea
LIP or continental slope
continental rise/abyssal
shoaling of CCD during OAE2
B
global marine carbonate content trends through OAE2
Carbonate content (wt.%)
0
10
20
30
40
50
60
70
80
90
100
pre-OAE2
OAE2
epicontinental sea
LIP or continental slope
continental rise/abyssal
shoaled CCD
sub-CCD throughout
above CCD throughout
CCD cutoff
W. Bermuda Rise, DSDP Site 387
Vigo Seamount, DSDP Site 398
US Atl. Cont. Rise, DSDP Site 603
Falkland Plateau, DSDP Site 511
Barnasiowka Section, Poland
NJ Margin, DSDP Site 105
C. Bermuda Rise, DSDP Site 386
Walvis Ridge, DSDP Site 530
Mentelle Basin, IODP Site U1513
Mentelle Basin, IODP Site U1516
Exmouth Plateau, ODP Site 763
Galicia Margin, ODP Site 641
Newfoundland Margin ODP Site 1276
Demerara Rise, ODP Site 1258
Rehkogelgraben, Austria
Furlo, Italy
Goban Spur, DSDP Site 549
Goban Spur, DSDP Site 551
Kerguelen Plat., ODP Site 1138
Exmouth Plateau, ODP Site 762
Blake Nose, ODP Site 1050
Bass River, NJ, USA
Angus Core, CO, USA
Grobern borehole, NW Europe
Tingri, Tibet
Pueblo, CO, USA
Olini & Paipa sections, Columbia
GM3 section, Jordan
Demerara Rise, ODP Site 1260
Oued Mellegue, Tunisia
Morocco Tarfaya SN4
Cuba, Kansas, USA
Pont Issole, France
Pulawy Borehole, Poland
Guerrero, Mexico platforms

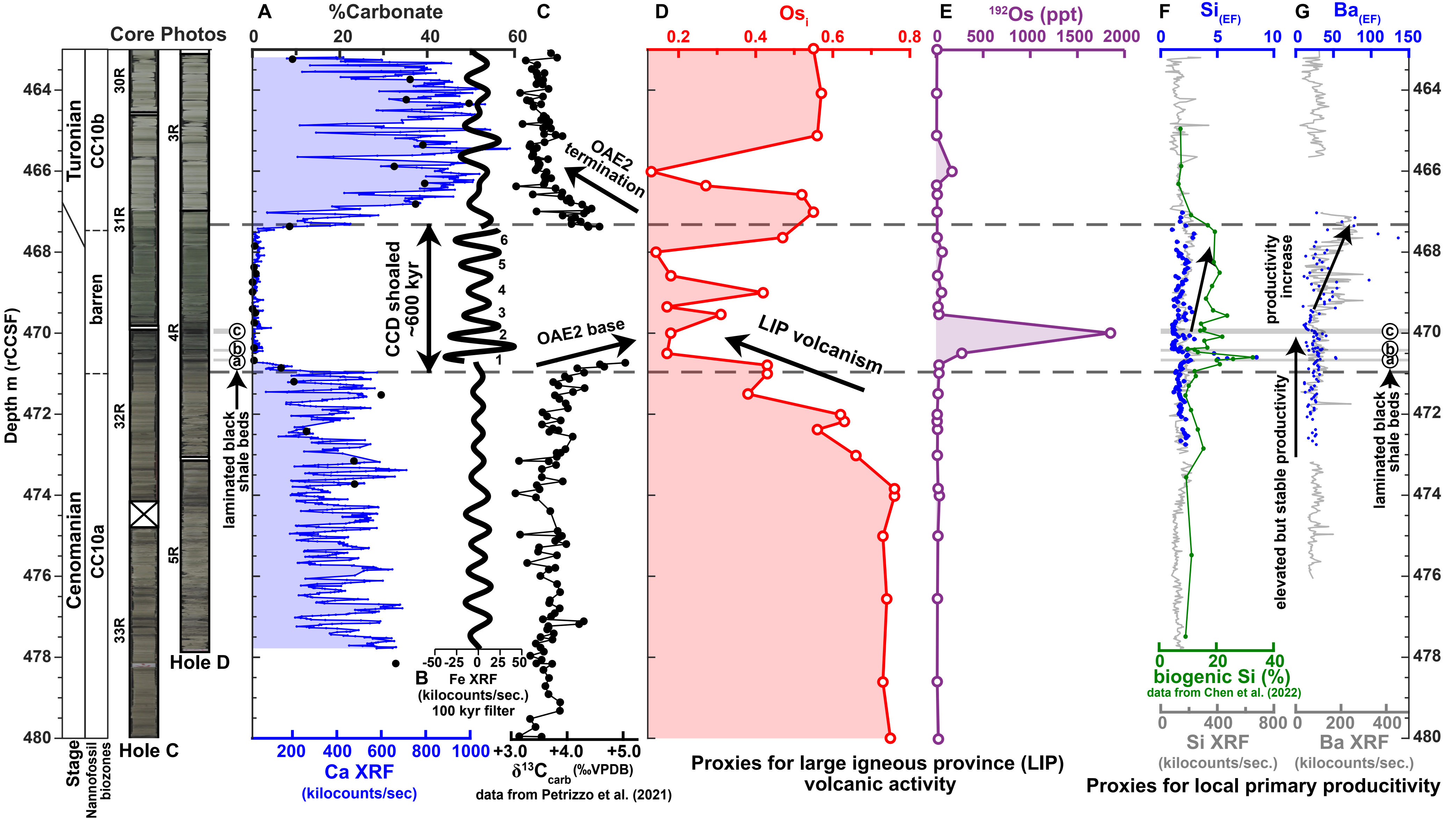
Core Photos
A
%Carbonate
0
20
40
60
C
D
Os$_i$
0.2
0.4
0.6
0.8
E
^{192}Os (ppt)
0
500
1000
1500
2000
F
Si$_{(EF)}$
0
5
10
G
Ba$_{(EF)}$
0
50
100
150
Depth m (rCCSF)
464
466
468
470
472
474
476
478
480
Turonian
Cenomanian
CC10b
barren
CC10a
30R
31R
32R
33R
3R
4R
5R
Stage
Nannofossil biozones
Hole C
Hole D
ⓒ
ⓑ
ⓐ
laminated black shale beds
CCD shoaled ~600 kyr
1
2
3
4
5
6
OAE2 termination
OAE2 base
LIP volcanism
productivity increase
elevated but stable productivity
laminated black shale beds
200
400
600
800
1000
Ca XRF (kilocounts/sec)
-50
-25
0
25
50
B
Fe XRF (kilocounts/sec.) 100 kyr filter
+3.0
+4.0
+5.0
δ^{13}C$_{carb}$ (‰VPDB)
data from Petrizzo et al. (2021)
Proxies for large igneous province (LIP) volcanic activity
0
20
40
biogenic Si (%)
data from Chen et al. (2022)
0
400
800
Si XRF (kilocounts/sec.)
0
200
400
Ba XRF (kilocounts/sec.)
Proxies for local primary producitivity

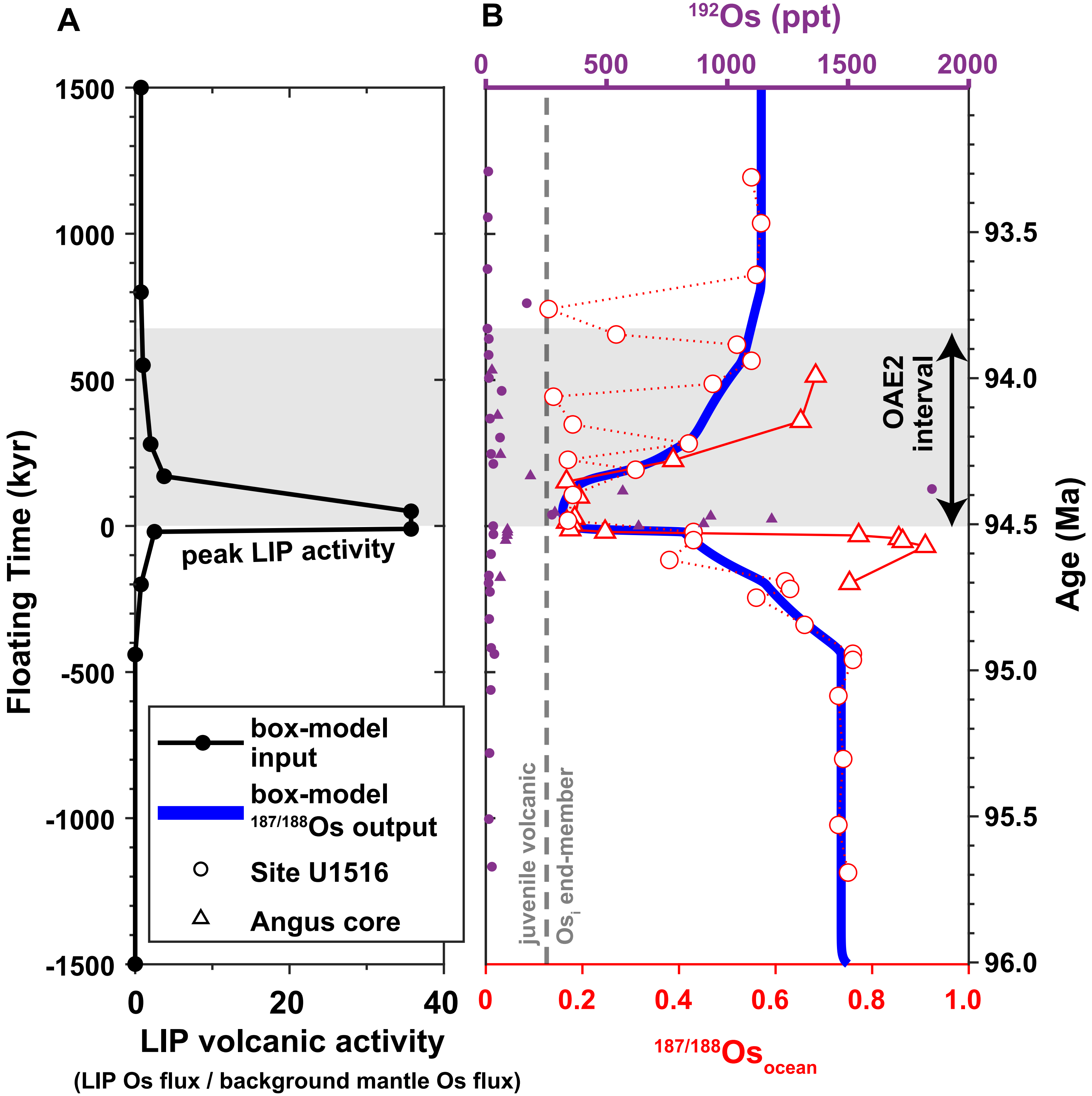
A
B
192Os (ppt)
0
500
1000
1500
2000
1500
1000
500
0
-500
-1000
-1500
Floating Time (kyr)
peak LIP activity
0
20
40
LIP volcanic activity
(LIP Os flux / background mantle Os flux)
box-model input
box-model 187/188Os output
Site U1516
Angus core
juvenile volcanic Osi end-member
OAE2 interval
93.5
94.0
94.5
95.0
95.5
96.0
Age (Ma)
0
0.2
0.4
0.6
0.8
1.0
187/188Os ocean

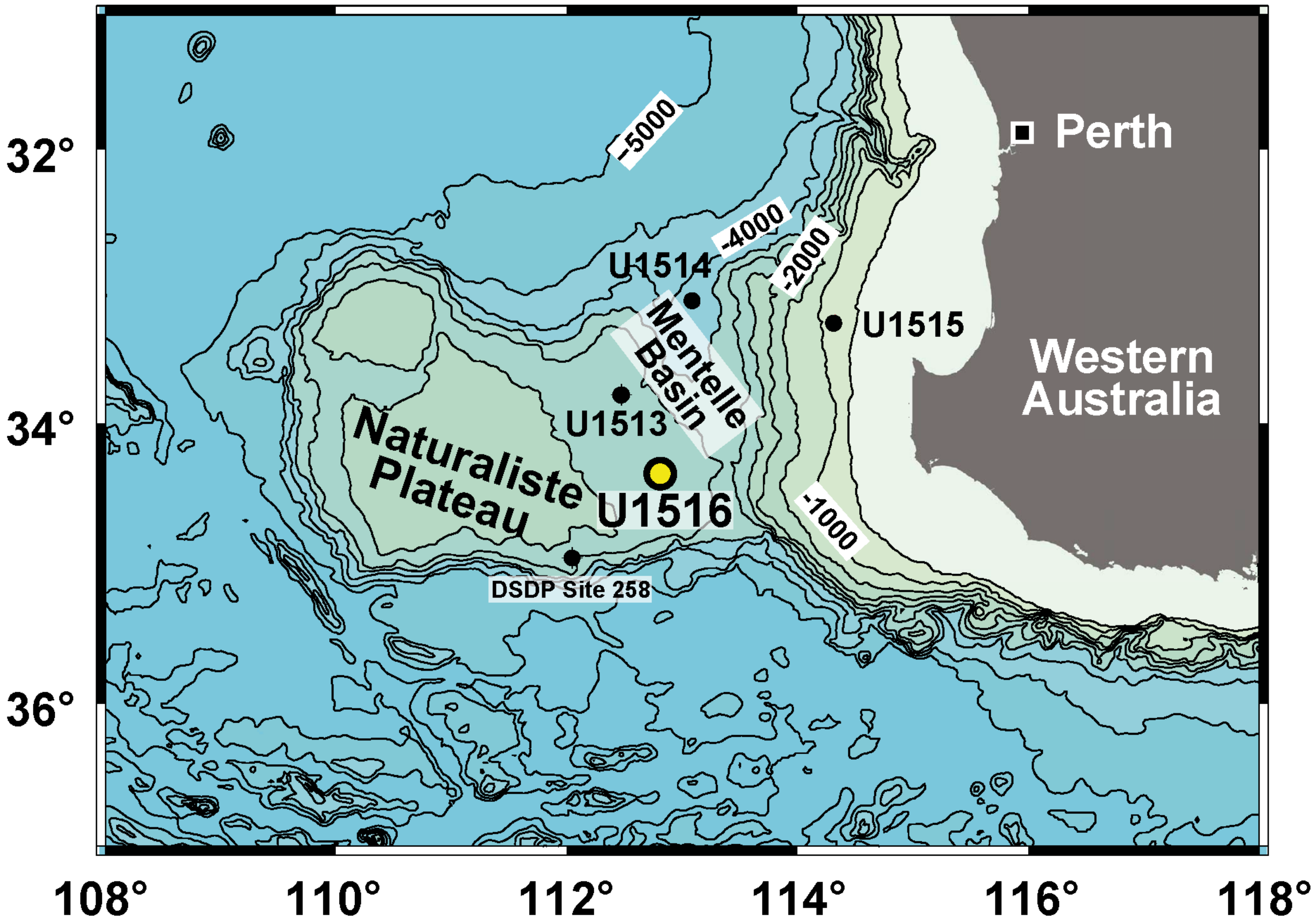
-5000
Perth
32°
-4000
-2000
U1514
U1515
Mentelle Basin
Western Australia
34°
U1513
Naturaliste Plateau
U1516
-1000
DSDP Site 258
36°
108°
110°
112°
114°
116°
118°

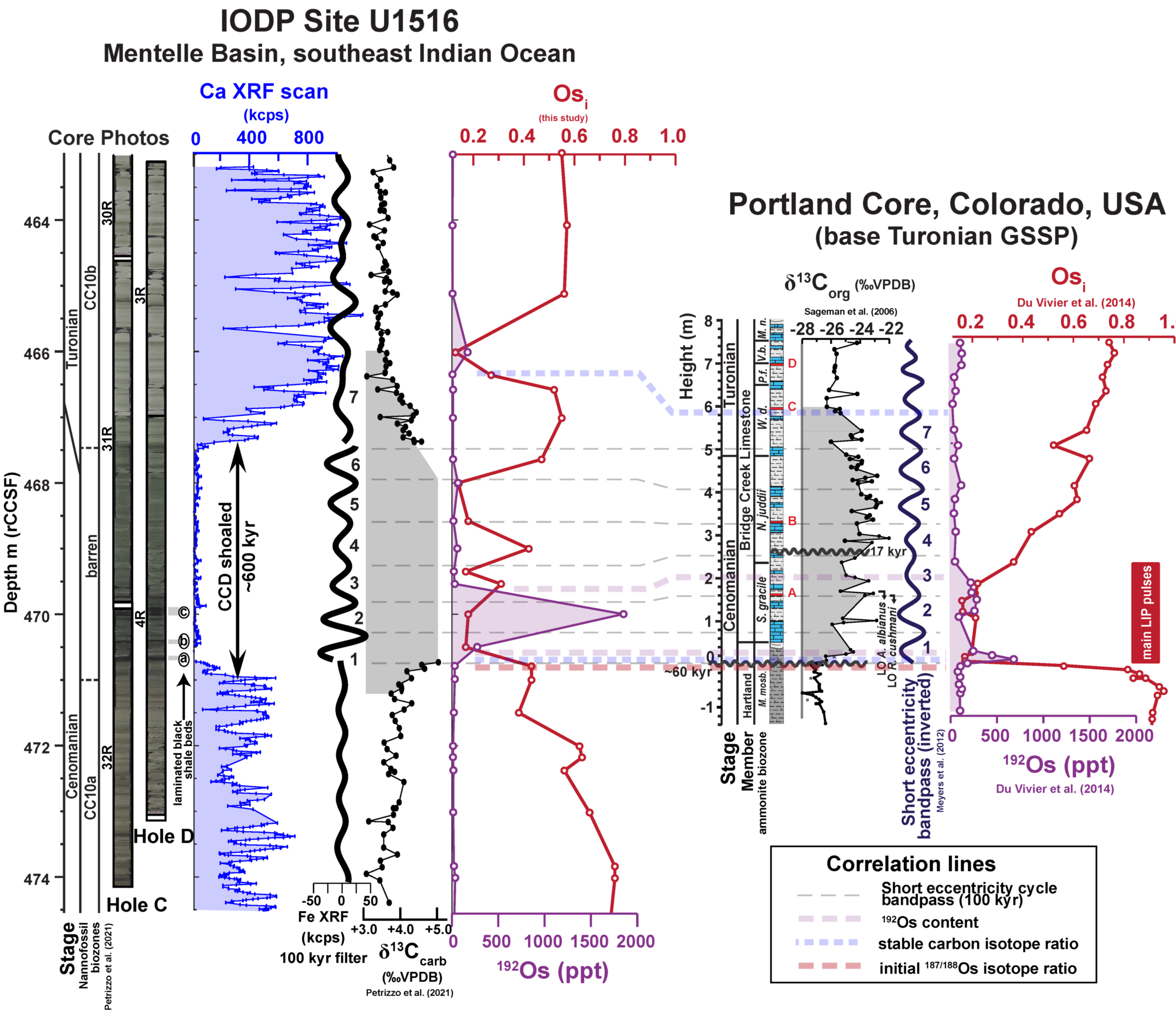
IODP Site U1516
Mentelle Basin, southeast Indian Ocean
Core Photos
Ca XRF scan
(kcps)
0
400
800
Osi
(this study)
0.2
0.4
0.6
0.8
1.0
Depth m (rCCSF)
464
466
468
470
472
474
Turonian
Cenomanian
CC10b
barren
CC10a
30R
31R
32R
3R
4R
Hole C
Hole D
Stage
Nannofossil biozones
Petrizzo et al. (2021)
laminated black shale beds
ⓐ
ⓑ
ⓒ
CCD shoaled
~600 kyr
1
2
3
4
5
6
7
-50
0
50
Fe XRF (kcps)
100 kyr filter
+3.0
+4.0
+5.0
δ13Ccarb (‰VPDB)
Petrizzo et al. (2021)
0
500
1000
1500
2000
192Os (ppt)
Portland Core, Colorado, USA
(base Turonian GSSP)
δ13Corg (‰VPDB)
Sageman et al. (2006)
-28
-26
-24
-22
Height (m)
8
7
6
5
4
3
2
1
0
-1
Turonian
Cenomanian
Bridge Creek Limestone
Hartland
M. n.
V. b.
P. f.
W. d.
N. juddii
S. gracile
M. mosb.
D
C
B
A
Stage
Member
ammonite biozone
17 kyr
~60 kyr
LO A. albianus
LO R. cushmani
Short eccentricity bandpass (inverted)
Meyers et al. (2012)
1
2
3
4
5
6
7
Osi
Du Vivier et al. (2014)
0.2
0.4
0.6
0.8
1.0
main LIP pulses
0
500
1000
1500
2000
192Os (ppt)
Du Vivier et al. (2014)
Correlation lines
Short eccentricity cycle bandpass (100 kyr)
192Os content
stable carbon isotope ratio
initial 187/188Os isotope ratio

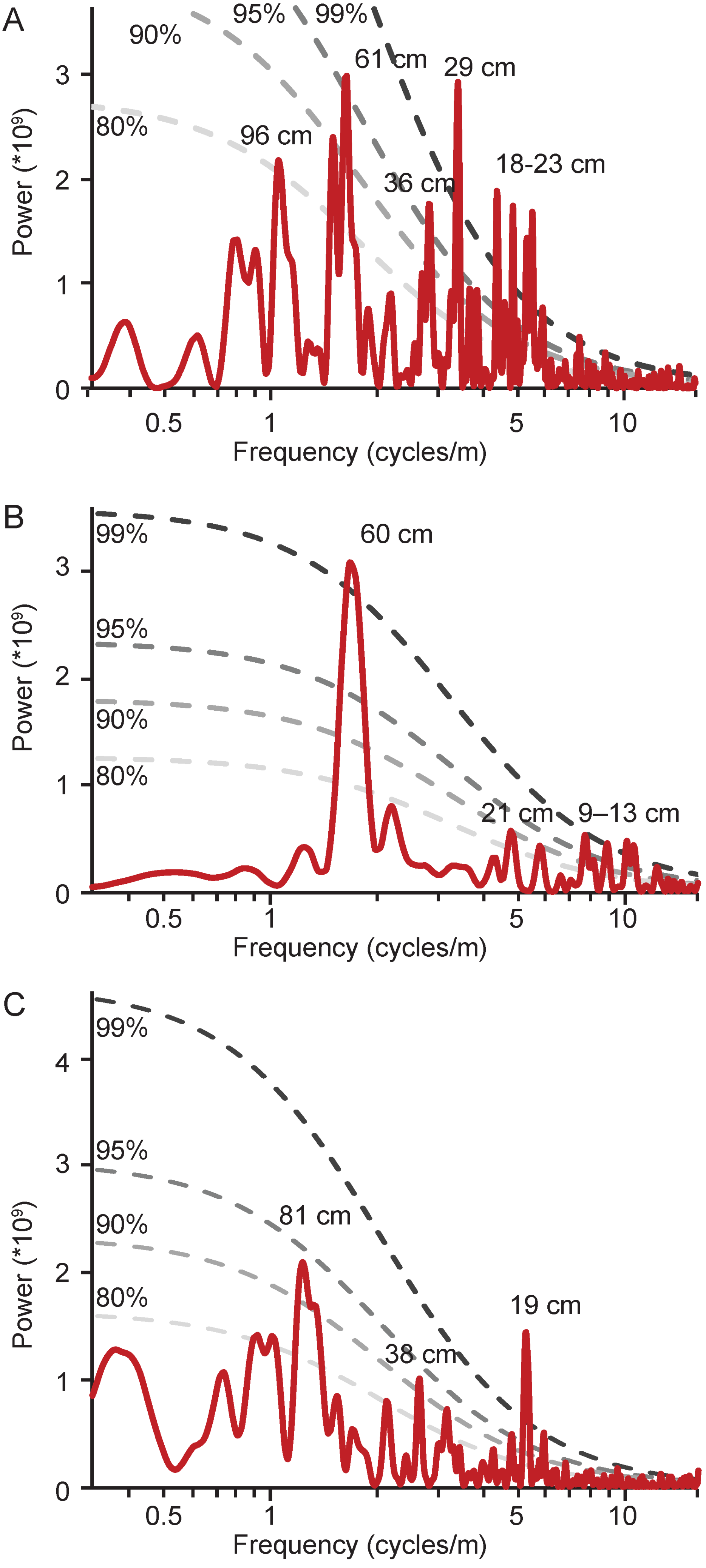
A
90%
95%
99%
80%
61 cm
29 cm
96 cm
36 cm
18-23 cm
Power (*10^9)
0
1
2
3
0.5
1
5
10
Frequency (cycles/m)
B
99%
95%
90%
80%
60 cm
21 cm
9–13 cm
Power (*10^9)
0
1
2
3
0.5
1
5
10
Frequency (cycles/m)
C
99%
95%
90%
80%
81 cm
38 cm
19 cm
Power (*10^9)
0
1
2
3
4
0.5
1
5
10
Frequency (cycles/m)

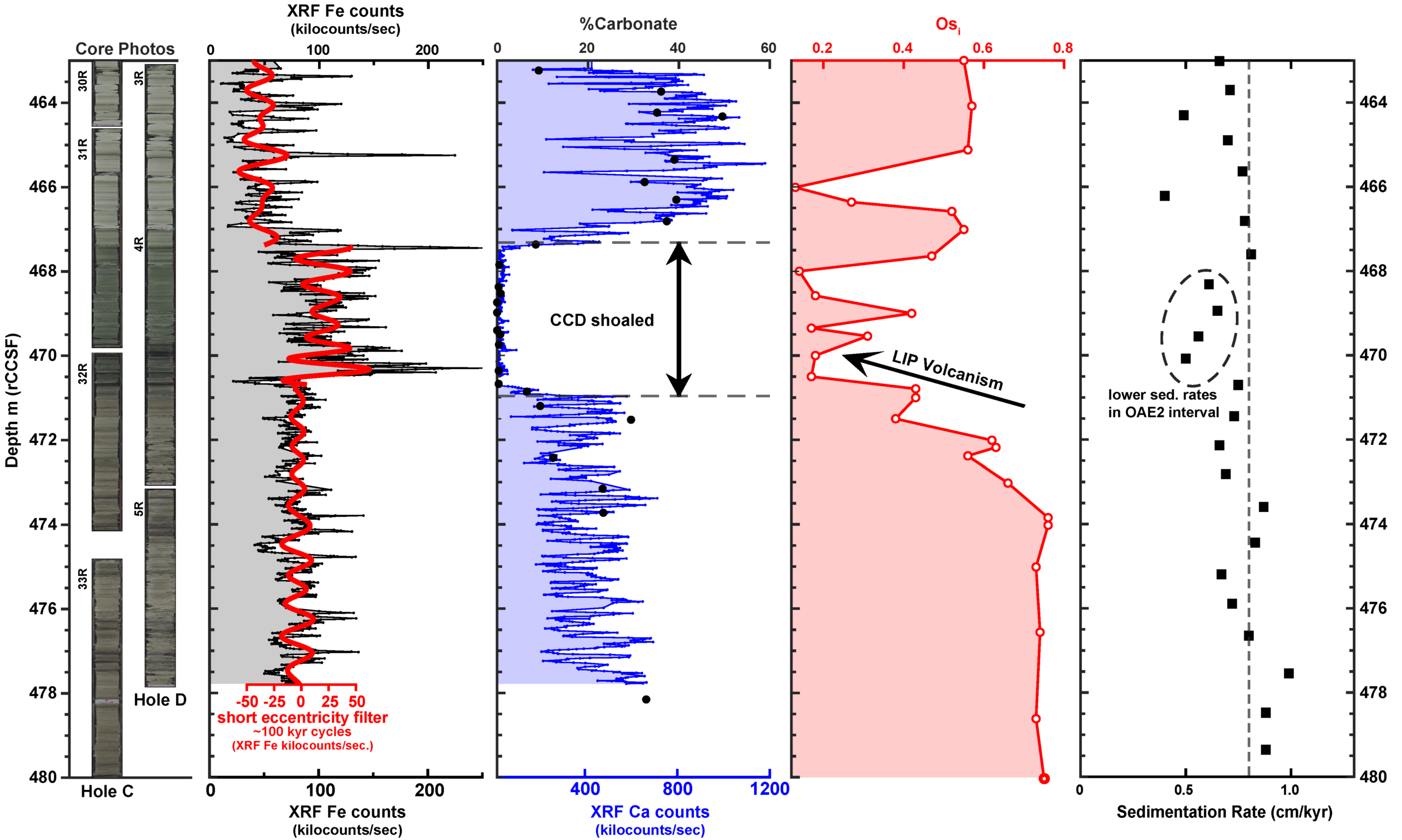
Core Photos
30R
31R
32R
33R
3R
4R
5R
Hole C
Hole D
Depth m (rCCSF)
464
466
468
470
472
474
476
478
480
XRF Fe counts
(kilocounts/sec)
0
100
200
-50 -25 0 25 50
short eccentricity filter
~100 kyr cycles
(XRF Fe kilocounts/sec.)
%Carbonate
0
20
40
60
CCD shoaled
400
800
1200
XRF Ca counts
(kilocounts/sec)
Os_i
0.2
0.4
0.6
0.8
LIP Volcanism
lower sed. rates
in OAE2 interval
0
0.5
1.0
Sedimentation Rate (cm/kyr)

A **SCENARIO 1: LIP VOLCANISM**

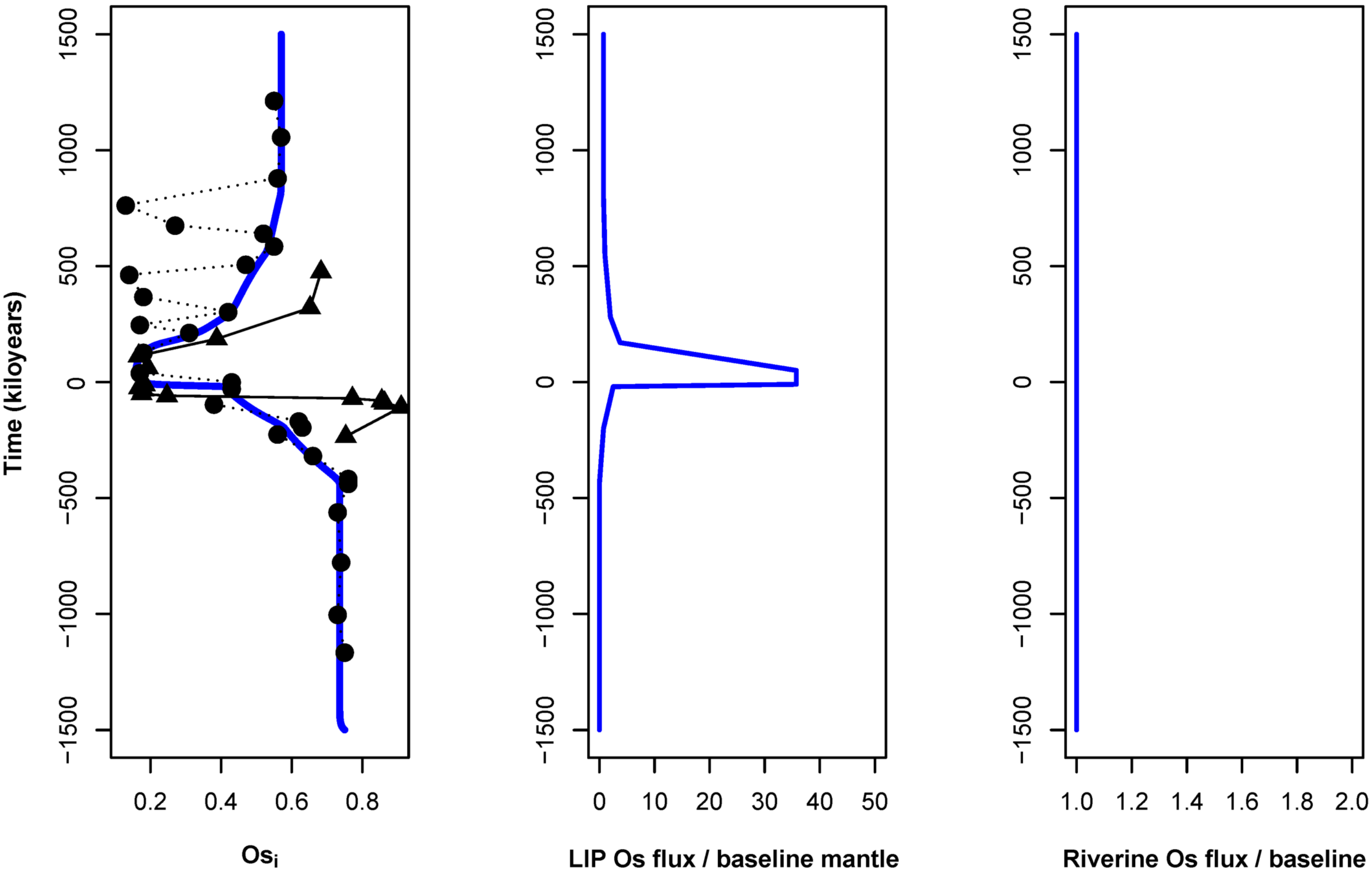

B **SCENARIO 2: LIP VOLCANISM + INCREASED CONTINENTAL WEATHERING**

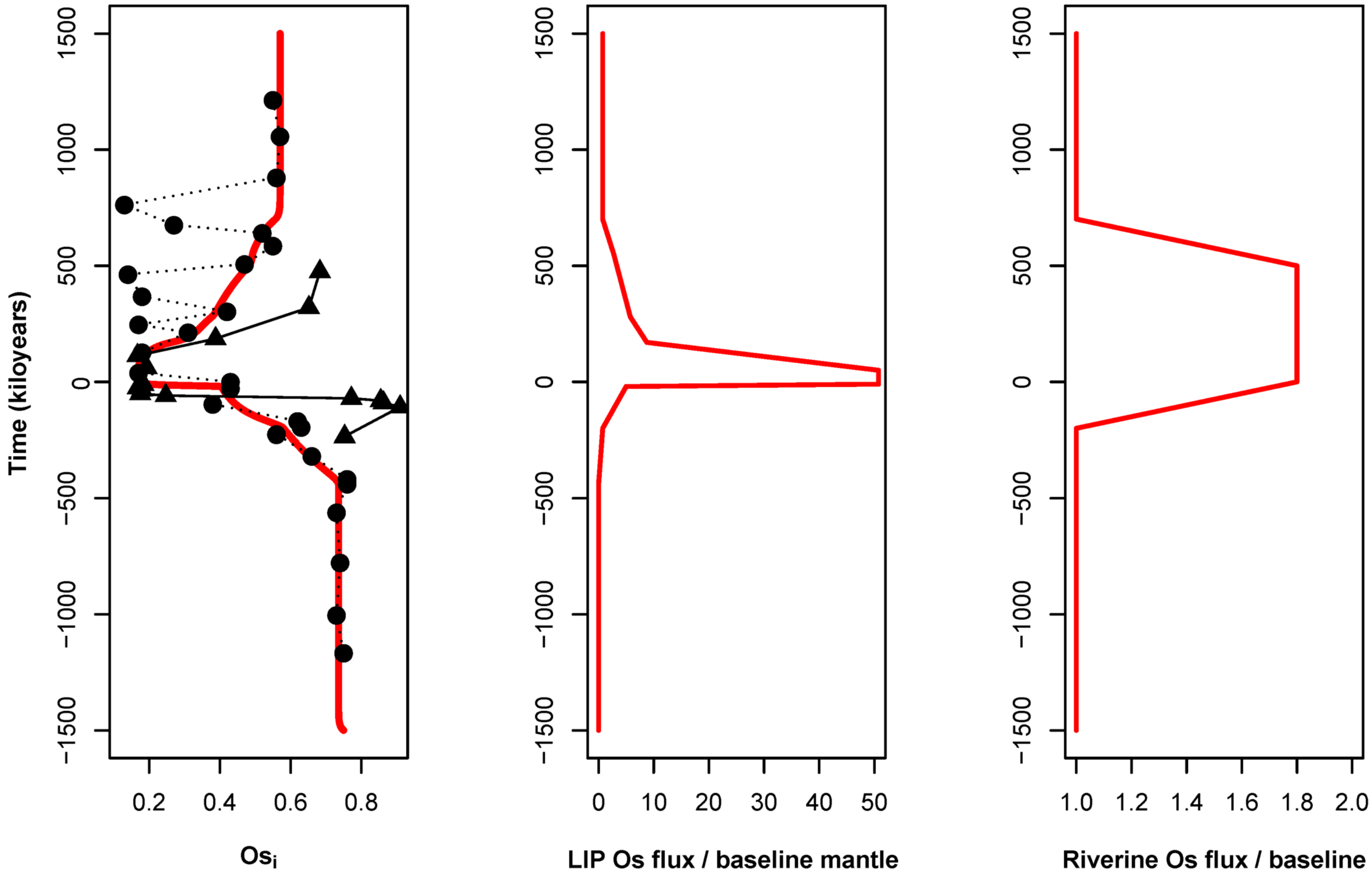

Marine Os Source/Sink	**$^{187/188}$Os (isotopic composition)**	**Flux (tonnes Os/kyr)**
Riverine (F_{riv})	1.4	339
Mantle/volcanic (F_{mantle})	0.126	352
Cosmic (F_{cosmic})	0.126	17.6
Large igneous province (F_{LIP})	0.126	iteratively varied*
Sedimentation (F_{sed})	Ro(t)	$M_o(t)/\tau$
Model Initial Conditions (t=0)	**Symbol**	**Value**
marine $^{187/188}$Os ratio	$R_o(0)$	0.9
mass of marine Os reservoir	$M_o(0)$	13,000 tonnes
marine Os residence time	τ	20,000 years

Floating time (kiloyears)	**LIP Os flux (F_{LIP}) (ratio: F_{LIP}/F_{mantle})**
1500	0.75
800	0.75
550	1
280	2
170	3.75
50	35.75
-10	35.75
-20	2.5
-200	0.75
-440	0
-1500	0

Site	Basin	Setting	pre-OAE2 %CaCO3	OAE2 %CaCO3	% change	CCD classification	Resolution of %carb record	References
W Bermuda Rise (DSDP Site 387)	proto-North Atlantic	Abyssal Plain	0	0	0%	sub-CCD	coarse	Tucholke et al. (1979)
Vigo Seamount (DSDP Site 398)	proto-North Atlantic	Seamount	0	0	0%	sub-CCD	coarse	Arthur (1979)
eastern N American Rise (DSDP Site 603)	proto-North Atlantic	Abyssal Plain	0	0	0%	sub-CCD	coarse	Meyers (1987) Dean and Arthur (1987)
New Jersey Margin (DSDP Site 105)	proto-North Atlantic	Continental Rise	7	7	0%	sub-CCD	high	Herbin et al. (1987)
Central Bermuda Rise (DSDP Site 386)	proto-North Atlantic	Continental Rise	15	9	-40%	sub-CCD	coarse	Cameron (1979) van Helmond et al. (2014)
Walvis Ridge (DSDP Site 530)	proto-South Atlantic	Abyssal Plain	15	20	33%	sub-CCD	high	Forster et al. (2008)
Falkland Plateau (DSDP Site 511)	proto-South Atlantic	Continental Slope	~0	~0	0%	sub-CCD	coarse	Huber et al. (1995)
Poland - Barnasiowka Section	Tethys?	Continental slope?	~0	~0	0%	sub-CCD	n/a	Uchman et al. (2008)
Mentelle Basin (IODP Site U1516)	proto-Indian Ocean	Continental Slope	25	0	-100%	shoaled CCD	high	Huber et al. (2019) Site U1516
Mentelle Basin (IODP Site U1513)	proto-Indian Ocean	Continental Slope	25	0	-100%	shoaled CCD	high	Huber et al. (2019) Site U1513
Exmouth Plateau (ODP Site 763C)	Tethys	Continental Slope	38	0	-100%	shoaled CCD	high	Thurow et al. (1992) Rullkötter et al. (1992)
Galicia Margin (ODP Site 641)	proto-North Atlantic	Continental Slope	40	0	-100%	shoaled CCD	high	Thurow et al. (1988) van Helmond et al. (2014)
Newfoundland Margin (ODP Site 1276)	proto-North Atlantic	Continental Rise	42	9	-79%	shoaled CCD	high	Shipboard Sci. Party (2004) Sinninghé Damste et al (2010) Arnaboldi and Meyers (2006)
Demerara Rise (ODP Site 1258)	proto-North Atlantic	Continental Slope	52	20	-62%	shoaled CCD?	high	Hetzel et al. (2009)
Austria - Rehkogelgraben Section	Tethys	Continental Slope	60	0	-100%	shoaled CCD	high	Wagreich et al. (2008)
Italy - Furlo section	Tethys	Continental Slope?	67	3	-97%	shoaled CCD	high	Turgeon & Burmsack (2006)
Goban Spur (DSDP Site 549)	proto-North Atlantic	Continental Slope	70	6	-91%	shoaled CCD	high	de Graciansky et al. (1985) Waples & Cunningham (1985) Linnert et al. (2011)
Goban Spur (DSDP Site 551)	proto-North Atlantic	Continental Slope	75	0	-100%	shoaled CCD	high	de Graciansky et al. (1985) Waples & Cunningham (1985) Linnert et al. (2011)
Exmouth Plateau (ODP Site 762)	Tethys	Continental Slope	76	0	-100%	shoaled CCD	coarse	Exon et al. (1992)
Kerguelen Plateau (ODP Site 1138)	proto-Indian Ocean	LIP Slope	77	4	-95%	shoaled CCD	high	Meyers et al. (2009) Dickson et al. (2017)
Blake Nose (ODP Site 1050)	proto-North Atlantic	Continental Slope	85	14	-84%	shoaled CCD	coarse	Huber et al. (1999)
Bass River, New Jersey (ODP Leg 174x/)	proto-North Atlantic	Epicontinental	10	25	150%	above CCD? Siliciclastic-rich, proximal	high	Bowman and Bralower (2005)
Colorado, USA Angus Core, Denver Basin	Western Interior Seaway	Epicontinental	45	65	44%	above CCD	high	Joo & Sageman (2014)
northwest Europe (Grobern borehole)	European Shelf Seas	Epicontinental	45	55	22%	above CCD	high	Voigt et al. (2006)
Gongzha, Tingri Tibet	Tethys	Epicontinental	50	70	40%	above CCD	high	Bomou et al. (2013)
Colorado, USA (Rock Canyon Anticline)	Western Interior Seaway	Epicontinental	50	65	30%	above CCD	high	Sageman et al. (2014)
Jordan (GM3 Section)	Tethys	Epicontinental	60	75	25%	above CCD	high	Wendler et al. (2010)
Columbia Olini & Paipa sections	La Luna Sea	Epicontinental	60	50	-17%	above CCD	high	Paez-Reyes et al. (2021)
Demerara Rise (ODP Site 1260)	proto-North Atlantic	Continental Slope	63	48	-24%	above CCD	high	Hetzel et al. (2009)
Tunisia Oued Mellegue area	Tethys	Epicontinental	70	80	14%	above CCD	high	Nederbragt & Fiorentino (1999)
Morocco (SN4 Core, Tarfaya Basin)	proto-North Atlantic	Epicontinental	70	75	7%	above CCD	high	Beil et al. (2018)
Kansas, USA (Cuba section)	Western Interior Seaway	Epicontinental	75	80	7%	above CCD	high	Bowman and Bralower (2005)
France (Lambruisse Section)	European Shelf Seas	Epicontinental	85	45	-47%	above CCD	high	Takashima et al. (2009)
Poland (Pulawy Borehole)	European Shelf Seas	Epicontinental	85	60	-29%	above CCD	coarse	Peryt & Wyrwicka (1993)
Guerrero state, Mexico carbonate platforms	Epicontinental Sea	Epicontinental	95	80	-16%	above CCD	high	Elrick et al. (2009)